Physics-constrained data-driven methods for chaotic flows. Part I.

Luca Magri*
University of Cambridge, Engineering Department, Trumpington St, Cambridge,
CB2 1PZ, United Kingdom

December 3, 2019

*lm547@cam.ac.uk

Contents

Abstract

About one hundred trillion bytes of data has been created in the world while reading this very sentence. The traditional triad of the scientific method–theory, experimentation and simulation–has added big data now. Central to big data science are artificial intelligence and machine learning, which are automated ways of transforming information into empirical knowledge.

Whereas empirical knowledge is crucial to many practical applications, such as facial recognition, empirical models do not necessarily fulfil physical principles, for example, conservation laws. Physical principles provide physical equations, which are essential to understanding, modelling and, ultimately, designing engineering systems that optimize a performance.

One of the most prominent engineering and scientific communities that has been working with big data and physical principles for decades is fluid mechanics. Fluid mechanics underpins many established and emerging world-wide industries as well as critical societal issues such as climate science and energy consumption. These problems involve flows that are unsteady, unpredictable and uncertain across a vast range of spatiotemporal scales. Because of this, numerical simulations and experimental measurements of the physics of fluids generate big data, which is to say that fluid mechanics is both a physical and big data discipline.

Machine learning models may not be interpretable, robust and generalizable, but they enable adaptive empirical modelling. On the other hand, physical principles are governed by "rigid equations", i.e., they do not adaptively change, but they are interpretable, robust and generalizable. Machine learning is excellent at finding correlations in big data, whereas human beings are excellent at extrapolating knowledge (physical principles). My research combines physical principles and empirical modelling into a unified approach: physics-constrained adaptive learning.

Preamble

This is an "alpha version". Therefore, sometimes different symbols and notations are used for the same quantity. Importantly, (i) vectors and matrices are written in bold fonts, except in Section 6 where they are written in italic fonts; (ii) an infinitesimal perturbation is denoted $\mathbf{x}'$ in Section 3, whereas it will be denoted $\delta\mathbf{x}$ in the remainder of the lecture; (iii) the matrix exponential is interchangeably denoted e and exp; and (iv) the inner product is interchangeably denoted $\langle\cdot,\cdot,\rangle$ and $[\cdot,\cdot,]$

You are very welcome to send feedback for improvement to lm547@cam.ac.uk.

Acknowledgement

I am grateful to postdoctoral fellow Dr Nguyen Anh Khoa Doan (Institute for Advanced Study, TU Munich) [1] and students Hans Yu (University of Cambridge) [2, 3], Francisco Huhn (University of Cambridge) [4] and Tullio Traverso (LadHyX, École Polytechnique) [5] for invaluable input. I acknowledge Dr Pablo Fernandez (Amazon) for helpful discussions on ergodic systems.

Some parts of this lecture are drawn on publications, which are acknowledged at the beginning of each section and in the figure captions.

1 Introduction

To predict how a flow, or any other physical system, evolves in space and time we need to find a model. One approach is to observe a small number of phenomena (relatively small data), find the variables, and an equation that connects the variables. This is called induction, which provides physical principles. Physical principles are extrapolative (until the assumptions upon which they hinge break down): they provide predictions on phenomena that have not been observed. Human beings are excellent at extrapolating

knowledge because we are excellent at finding physical principles. A different approach is to observe a large number of phenomena (big data), identify the inputs and outputs, and a function that connects them. This is called empirical modelling, which provides correlation functions. Artificial intelligence and machine learning are excellent at finding correlations in big data. Once a model is created, we can manipulate the equations to deduce new phenomena. This is called deduction, which provides further extrapolative knowledge. In this project, we will enhance extrapolative models by infusing physical principles into artificial intelligence and machine learning algorithms.

1.1 The three big U's of fluid mechanics

A flow that interacts with other physical systems, such as chemical reactions and structures, is a multi-physics problem. We will call it multi-physics flow for brevity. Here, we are interested in *nonlinear multi-physics flows* that are

- unsteady
- unpredictable
- uncertain

I will sometimes call these the *three big U's of fluid mechanics*. Let us have a look at why these flows are intractable by explaining each U in the 3U. Many multi-physics flows oscillate because they are linearly unstable in time. These unsteady dynamics become unpredictable when the flow becomes turbulent. Turbulent flows are chaotic dynamical systems, which are extremely sensitive to small perturbations to the system (butterfly effect). Because of the butterfly effect, the time accurate prediction of chaotic flows can only be guaranteed for a short time, which is called the predictability time. After the predictability time, a minuscule difference between the initial conditions, such as floating-point errors, is exponentially amplified, which results in completely different instantaneous solutions. The butterfly effect generates a deterministic uncertainty. Within the predictability time the deterministic uncertainty is small, but the flow dynamics is still uncertain due to random disturbances, which originate from external noise, unknown variations (or miscalibration) of the parameters, and the action of hidden physical variables that are not captured in the model. This randomness generates stochastic uncertainties. In multi-physics flows, the nonlinear interactions propagate the uncertainty across the different subsystems in an intricate way. Both deterministic and stochastic uncertainties make the time and spatial prediction of a multi-physics flow challenging. This is a roadblock for the robust optimization of chaotic multi-physics flows, which is still an open scientific and industrial problem. The question is "how can we optimize multi-physics flows that are unsteady, unpredictable and uncertain with affordable computations?" This lecture provides some tools to tackle these questions.

1.2 Machine learning and empirical modelling in fluid mechanics

Fluid mechanics is one of the original big data communities. Big data is produced by computational fluid dynamics simulations with up to billions of degrees of freedom, and by high-resolution experimental measurements. Examples of machine learning applications to fluids are flow feature extraction for reduced-order modelling; dimensionality reduction; classification of wake topology; sparse compressing sensing for representation of wall bounded turbulence; trajectory analysis and classification of particle image velocimetry; reconstruction of turbulence flow fields; identification of coherent structures from time-series data; flow optimization for turbines; super-reconstruction of high-resolution fields; and many other applications, for example, reinforcement learning and sparse identification [6, 7, 8]. These fluids applications are mostly data driven, i.e., physical principles are not enforced in the machine learning algorithms, except for simplified problems and for learning turbulence closure models. Machine learning techniques have been applied to simplified problems with success, but we still do not know if, and how, they can be used as predictive and optimization tools for multi-physics engineering flows.

1.2.1 Physics-constrained learning: making the most out of empirical modelling and physical principles

On the one hand, fully-data driven machine learning models may not be interpretable, robust and generalizable, but they enable versatile adaptive empirical modelling. On the other hand, physical principles provide "rigid equations", i.e., they do not adaptively change (they do not learn) any time that new data is available, but they are interpretable, robust and generalizable. Here, we will show how to combine physical principles and empirical modelling. To combine physical principles with empirical modelling by machine learning, which are two radically different approaches, into a consistent framework, we exploit multi-disciplinary tools: (i) dynamical systems theory, in particular chaos theory, to tackle unsteadiness and unpredictability; (ii) Bayesian statistical inference, in particular data assimilation from weather forecasting, to work with uncertainty; (iii) optimization, in particular constrained optimization with adjoint methods, to maximize (or minimize) time-averaged cost functionals.

1.3 Objectives

1. Show how to combine physical principles with machine learning.
2. Explain how to create adaptive models by on-the-fly assimilation of experimental measurements.
3. Accompany the predictions with robust uncertainty quantification.

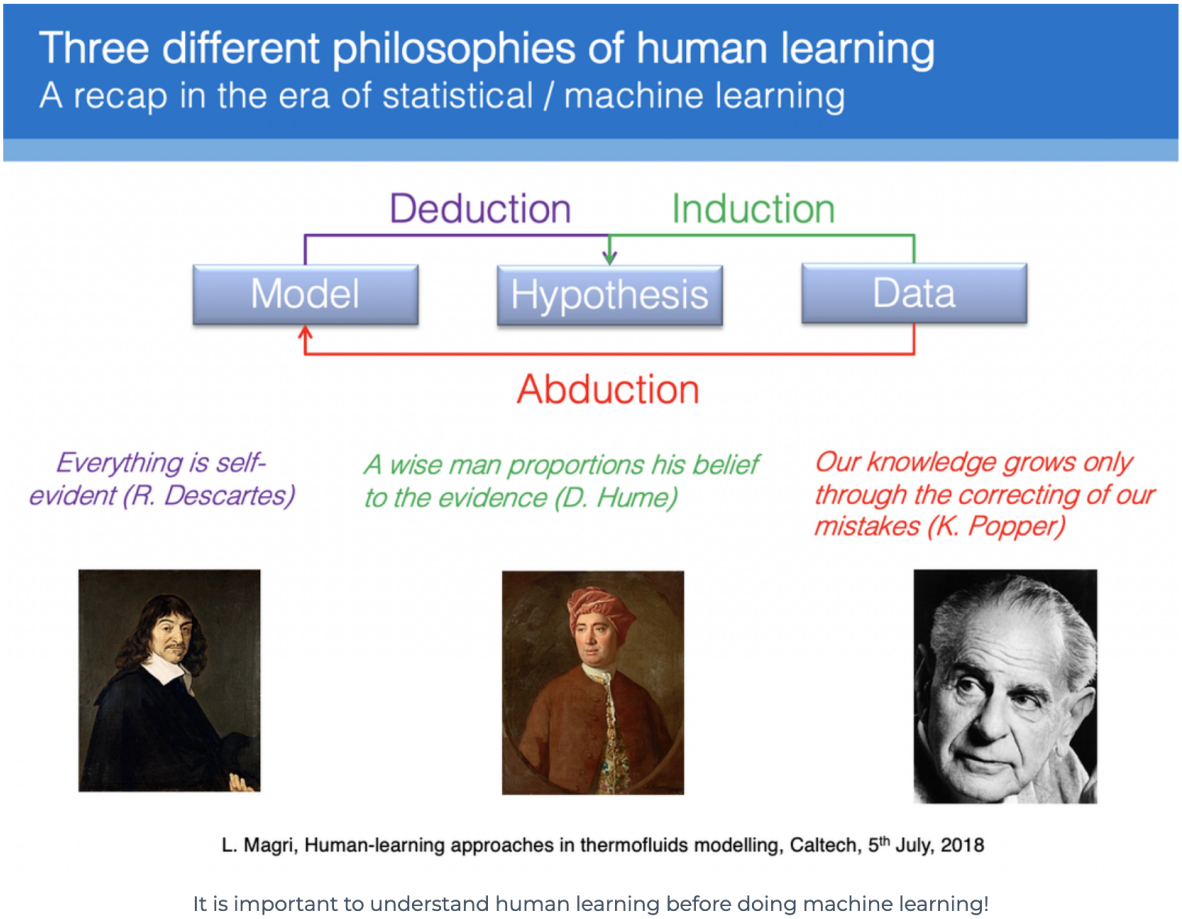

Figure 1: Yes, it is important to understand human learning before doing machine learnig!

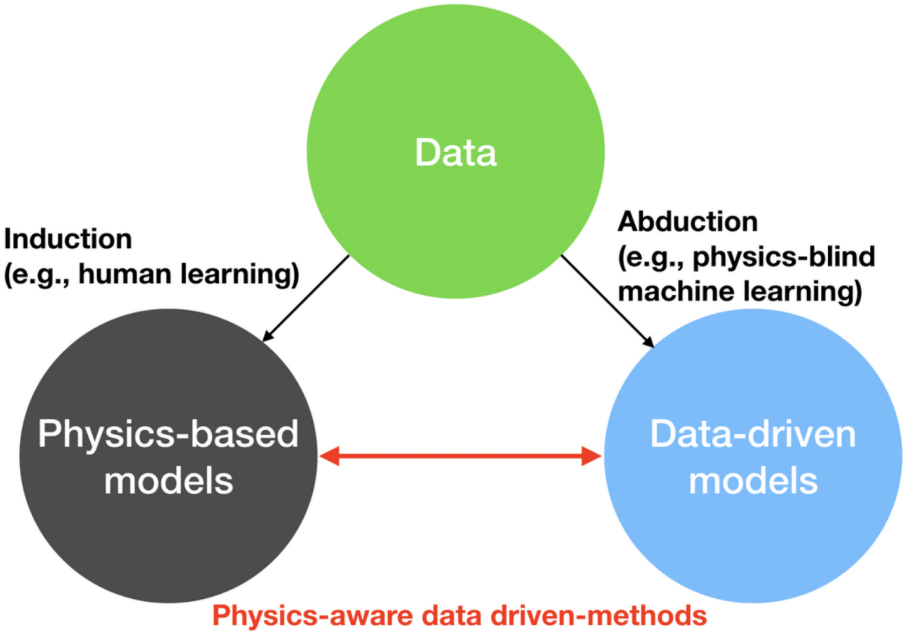

Figure 2: Reduced-order models are practical tools but they have parameter/model uncertainties. High-fidelity simulations are accurate tools but they cannot time-accurately capture rare/extreme events. Data driven methods help combine data with models, but we ought not to forget the physical constraints.

2 Deterministic nonlinear system

We assume that the multi-physics fluid dynamics problem is governed by partial differential equations, i.e. the compressible Navier-Stokes equation with equations for the chemistry, and mass and energy conservation. After spatial discretisation, the problem is an autonomous dynamical system

$$\begin{cases} \dot{\mathbf{x}}(t) = \boldsymbol{F}(\mathbf{x}(t), \mathbf{p}) \\ \mathbf{x}(0) = \mathbf{x}_0 \end{cases} \tag{1}$$

where the overdot $\dot{(\,)}$ is Newton's notation for time differentiation; $\mathbf{x} \in \mathbb{R}^N$ is the state vector (e.g. pressure and velocity at each discrete location), where the integer N denotes the discrete degrees of freedom; the subscript 0 denotes the initial condition; $\boldsymbol{F} : \mathbb{R}^N \to \mathbb{R}^N$ is a nonlinear smooth function, which encapsulates the discretised boundary conditions; and $\mathbf{p}$ is a vector containing the system's parameters, which will be dropped unless it is necessary for clarity. If we are interested in the evolution of infinitesimal perturbations, we split the solution as

$$\mathbf{x}(t) = \bar{\mathbf{x}}(t) + \mathbf{x}'(t), \tag{2}$$

where $\bar{\mathbf{x}}(t)$ is the unperturbed solution of (1) such that $||\bar{\mathbf{x}}'(t)||/||\bar{\mathbf{x}}(t)|| \sim O(\epsilon)$, where $\epsilon \to 0$. The perturbation is governed by the tangent equation

$$\begin{cases} \dot{\mathbf{x}}' = \boldsymbol{J}(t)\mathbf{x}', \\ \mathbf{x}'(0) = \mathbf{x}'_0, \end{cases} \tag{3}$$

where

$$\boldsymbol{J}(t) \equiv \frac{d\boldsymbol{F}}{d\mathbf{x}}\Big|_{\bar{\mathbf{x}}(t)} \tag{4}$$

is the Jacobian.

3 Dynamical systems and chaos: Lyapunov analysis

Parts of this section are adapted from [1, 4].

Turbulent flows are chaotic flows. As such, the space-and-time accurate prediction of the solution is difficult to achieve because of the butterfly effect [9]: Two nearby initial conditions, which can differ by a very small amount, will practically diverge in time from each other with an exponential rate. This divergence rate is the dominant Lyapunov exponent. Whereas the statistics of turbulent flows may not be significantly affected by tiny perturbations, the instantaneous solution is. (Having accurate predictions on the instantaneous solution is crucial for the prediction of rare and transient events.) For example, running the same code with the same initial conditions on a different number of processors should in principle provide two statistically equivalent solutions, but with completely different instantaneous fields after a few time steps.
Albeit the butterfly effect seems to be a showstopper for the time-accurate prediction of turbulent flows, such a prediction can be greatly aided by physics-informed data-driven methods. Dynamical systems theory provides the predictability of a chaotic simulation, which is the time scale after which the trajectories diverge due to the butterfly effect.
There exist different approaches to characterize a chaotic solution [10, 11, 12]. The dominant Lyapunov exponent is a practical measure to compute the predictability of large scale simulations because it (i) is easy to calculate [12] and (ii) does not depend on the initial conditions in ergodic processes [13]. In large scale fluid-dynamics simulations, the Lyapunov exponent was calculated in channel and bluff-body flows [14], homogeneous isotropic turbulence [15, 16], reacting and non-reacting turbulent jets [15], a two-dimensional airfoil [17], backward-facing step [18], partially-premixed flames [19], to name only a few.

3.1 Covariant Lyapunov vector analysis

This section introduces the key concepts to perform stability and sensitivity analysis of chaotic systems. In particular, we present the key results of Oseledets' theorem [20] to lay out the fundamentals of covariant Lyapunov vector analysis [21]. (Note that covariant Lyapunov vector analysis has nothing to do with Lyapunov stability analysis based on Lyapunov functions, which is used, for example, in control theory.)

3.1.1 Lyapunov exponents

To define the Lyapunov exponents, referring to (1), (3), it is convenient to introduce the tangent propagator, which maps the perturbation, $\mathbf{x}'$, from time t to time $\tilde{t}$, as

$$\mathbf{x}'(t+\tilde{t}) = \boldsymbol{M}(t,\tilde{t})\mathbf{x}'(t). \tag{5}$$

The tangent propagator is governed by the matrix equation

$$\begin{cases} \frac{d\boldsymbol{M}}{d\tilde{t}} = \boldsymbol{J}(\tilde{t})\boldsymbol{M}, \\ \boldsymbol{M}(t,0) = \boldsymbol{I}, \end{cases} \tag{6}$$

where $\boldsymbol{I}$ is the identity matrix. Setting $t = 0$ without loss of generality, the norm of an infinitesimal perturbation, $\mathbf{x}'_0$, to the initial condition, $\bar{\mathbf{x}}_0$, asymptotically grows (or decays) as

$$||\mathbf{x}'(\tilde{t})|| \cong ||\mathbf{x}'_0|| e^{\lambda(\mathbf{x}'_0,\bar{\mathbf{x}}_0)\tilde{t}}, \tag{7}$$

where $\cong$ means "asymptotically equal to", and

$$\lambda(\mathbf{x}'_0,\bar{\mathbf{x}}) = \lim_{\tilde{t}\to\infty} \frac{1}{\tilde{t}} \log \frac{||\boldsymbol{M}(0,\tilde{t})\mathbf{x}'_0||}{||\mathbf{x}'_0||} \tag{8}$$

is the characteristic Lyapunov exponent.

3.1.2 Oseledets' theorem

Oseledets' theorem [20] shows that there exist $m \leq N$ distinct Lyapunov exponents $\lambda_1(\bar{\mathbf{x}}) > \lambda_2(\bar{\mathbf{x}}) > \cdots > \lambda_m(\bar{\mathbf{x}})$, which provide a filtration of the tangent space $\mathcal{T}_{\bar{\mathbf{x}}}$, into subspaces S_i, i.e. $\mathcal{T}_{\bar{\mathbf{x}}} \equiv S_1 \supset S_2 \supset \cdots \supset S_m$, such that $\mathbf{x}_0' \in S_j \backslash S_{j+1} \Leftrightarrow \lambda(\mathbf{x}_0', \bar{\mathbf{x}}) = \lambda_j(\bar{\mathbf{x}})$. Furthermore, Oseledets' theorem shows that $\lambda_j(\bar{\mathbf{x}})$ are constants of the attractor $\bar{\mathbf{x}}$, and, in ergodic systems, λ_j do not depend on the initial condition, $\bar{\mathbf{x}}_0$. Physically, the Lyapunov exponents are the average exponential contraction/expansion rates of an infinitesimal volume of the phase space moving along the attractor.

3.1.3 Oseledets splitting and covariant Lyapunov vectors

The Lyapunov exponents are invariant measures of the attractor, however, they do not inform on the directions along which the infinitesimal volume of the phase space contracts/expands. Such directions are provided by the Oseledets splitting, which is composed by the Lyapunov subspaces, which are, in turn, spanned by the covariant Lyapunov vectors. First, the Oseledets matrix [20] is defined as

$$\boldsymbol{\Xi}^{\pm}(t) = \lim_{\tilde{t} \to \pm\infty} \frac{1}{2\tilde{t}} \log \left[\boldsymbol{M}(t, \tilde{t})^T \boldsymbol{M}(t, \tilde{t}) \right]. \tag{9}$$

This matrix is called "forward" if $\tilde{t} \to +\infty$ or "backward" if $\tilde{t} \to -\infty$. The spectrum of this matrix contains $m \leq N$ distinct eigenvalues, which are the Lyapunov exponents of the system $\lambda_1 > \lambda_2 > \cdots > \lambda_m$. However, the eigenvectors of the forward and backward matrices differ from each other and are not invariant under time reversal.

More insight into the Oseledets matrix. Consider the singular value decomposition $\boldsymbol{M}(t, \tilde{t}) = \boldsymbol{U}\boldsymbol{\Sigma}\boldsymbol{V}^T$, where $\boldsymbol{U}$ and $\boldsymbol{V}$ are orthogonal matrices and $\boldsymbol{\Sigma}$ is a diagonal matrix with non-negative real entries (the singular values). We can obtain an eigenvalue decomposition of the argument of the logarithm of (9), $\boldsymbol{M}^T\boldsymbol{M} = \boldsymbol{V}(\boldsymbol{\Sigma}^T\boldsymbol{\Sigma})\boldsymbol{V}^T = \boldsymbol{V}\boldsymbol{\Sigma}^2\boldsymbol{V}^T$, which, after applying the logarithm, becomes $\boldsymbol{V}\log(\boldsymbol{\Sigma}^2)\boldsymbol{V}^T = 2\boldsymbol{V}\log(\boldsymbol{\Sigma})\boldsymbol{V}^T$. Thus, equation (9) can be rewritten as $2\boldsymbol{\Xi}^{\pm}(t) = \lim_{\tilde{t}\to\pm\infty} \boldsymbol{V}(\log(\boldsymbol{\Sigma}(t, \tilde{t}))/\tilde{t})\boldsymbol{V}^T$, which shows that the eigenvalues of $\boldsymbol{\Xi}^{\pm}$ are the Lyapunov exponents, which are equal to the exponential average of the singular values of $\boldsymbol{M}(t, \tilde{t})$.

Let $V_j^{\pm}(t)$ be the j-th eigenspace of the forward (backward) Oseledets matrix, then the Oseledets subspaces are defined as

$$\Gamma_j^+(t) = V_j^+(t) \oplus \cdots \oplus V_m^+(t), \tag{10}$$

$$\Gamma_j^-(t) = V_1^-(t) \oplus \cdots \oplus V_j^-(t), \tag{11}$$

where $\oplus$ is the direct sum. The Oseledets subspaces have the property

$$\lim_{\tilde{t}\to\infty} \frac{1}{\tilde{t}} \log \frac{||\boldsymbol{M}(t, \tilde{t})\mathbf{x}'(t)||}{||\mathbf{x}'(t)||} = \lambda_j, \quad \text{for } \mathbf{x}'(t) \in \Gamma_j^{\pm}(t) \backslash \Gamma_{j+1}^{\pm}(t) \tag{12}$$

and a nested structure $\mathbb{R}^N = \Gamma_1^+(t) \supset \Gamma_2^+(t) \supset \cdots \supset \Gamma_m^+(t) \supset \Gamma_{m+1}^+(t) \equiv \emptyset$ and $\mathbb{R}^N = \Gamma_m^-(t) \supset \Gamma_{m-1}^-(t) \supset \cdots \supset \Gamma_1^-(t) \supset \Gamma_0^-(t) \equiv \emptyset$. By intersecting the Oseledets subspaces, we obtain the Lyapunov subspaces

$$\Omega_j(t) = \Gamma_j^+(t) \cap \Gamma_j^-(t), \quad j \in \{1, \ldots, m\}, \tag{13}$$

which compose the Oseledets splitting. The Lyapunov subspaces are (i) generally non-orthogonal to each other, (ii) covariant with the dynamics, i.e. $\boldsymbol{M}(t, \tilde{t})\Omega_j(t) = \Omega_j(t + \tilde{t})$, and (iii) invariant under time reversal. Each vector $\boldsymbol{\phi}_j(t)$ of a set that spans one of the Lyapunov subspaces is a covariant Lyapunov

vector associated with the Lyapunov exponent λ_j. If a trajectory is infinitesimally perturbed at some time t_1 along a covariant Lyapunov vector, the perturbation will grow at an exponential rate dictated by the associated Lyapunov exponent and will stay aligned with that same covariant Lyapunov vector (figure 3).

We derive the equation that governs the covariant Lyapunov vectors. First, because the Lyapunov subspaces are covariant with the dynamics, the following definition holds

$$\boldsymbol{M}(t,\tilde{t})\boldsymbol{\phi}(t) = \eta(t,\tilde{t})\boldsymbol{\phi}(t+\tilde{t}), \tag{14}$$

$$\text{where} \qquad \boldsymbol{M}(t,\tilde{t}) = \mathcal{P}\left(\exp\left(\int_t^{t+\tilde{t}} \boldsymbol{J}(\chi)d\chi\right)\right), \tag{15}$$

where $\eta(t,\tilde{t})$ is a scalar that measures the asymptotic growth of the norm and allows $\boldsymbol{\phi}(t+\tilde{t})$ to have any desired bounded norm, and $\mathcal{P}\left(\exp\left((\cdot)\right)\right)$ is the path-ordered exponential (appendix A). Substituting (15) in (14) and differentiating with respect to $\tilde{t}$ results in

$$\boldsymbol{J}(t+\tilde{t})\mathcal{P}\left(\exp\left(\int_t^{t+\tilde{t}} \boldsymbol{J}(\chi)d\chi\right)\right)\boldsymbol{\phi}(t) = \frac{d\eta(t,\tilde{t})}{d\tilde{t}}\boldsymbol{\phi}(t+\tilde{t}) + \eta(t,\tilde{t})\frac{d\boldsymbol{\phi}(t+\tilde{t})}{d\tilde{t}}. \tag{16}$$

By setting $t=0$ and omitting the explicit dependence on $t=0$, we obtain

$$\frac{d\boldsymbol{\phi}}{d\tilde{t}} = \boldsymbol{J}(\tilde{t})\boldsymbol{\phi}(\tilde{t}) - \frac{1}{\eta(\tilde{t})}\frac{d\eta(\tilde{t})}{d\tilde{t}}\boldsymbol{\phi}(\tilde{t}), \tag{17}$$

for any $\eta(\tilde{t}) \neq 0$. Moreover, we know from Oseledets' theorem that

$$\left|\left|\boldsymbol{M}(\tilde{t})\boldsymbol{\phi}(0)\right|\right| \cong e^{\lambda\tilde{t}}||\boldsymbol{\phi}(0)||, \tag{18}$$

which shows that $\eta(\tilde{t}) \cong e^{\lambda\tilde{t}}$. If we choose to have a bounded non-zero covariant Lyapunov vector, i.e. $0 < ||\boldsymbol{\phi}|| < \infty$, (17) becomes

$$\frac{d\boldsymbol{\phi}}{d\tilde{t}} = \boldsymbol{J}\boldsymbol{\phi} - \lambda\boldsymbol{\phi}. \tag{19}$$

It is easier to mathematically manipulate and numerically solve (19) than (13). Moreover, equation (19) provides a clear picture of the evolution of a covariant Lyapunov vector: the vector is evolved by the tangent dynamics $\boldsymbol{J}\boldsymbol{\phi}$, while the extra term $-\lambda\boldsymbol{\phi}$ guarantees that its norm is bounded. It can be shown that if the attractor is periodic or chaotic, there is a neutral mode ($\lambda = 0$), where $\boldsymbol{\phi}$ is collinear to $\dot{\bar{\mathbf{x}}}$ [22]. In the remainder of this paper, $t=0$ without loss of generality and the tilde, $\tilde{()}$, is dropped for brevity.

3.2 Numerical computation of Lyapunov exponents and covariant Lyapunov vectors

We use a robust algorithm [23, 21], called the QR algorithm for brevity, to calculate the Lyapunov spectrum and covariant vectors. The algorithm evolves a set of m column vectors $\boldsymbol{g}_j$, $j = \{1,\dots,m\}$ of an $N \times m$ matrix $\boldsymbol{M}$, via the tangent equation (6). Because the $\boldsymbol{g}_j$ will likely have a component in the most unstable (least stable) space Ω_1, their norm will exponentially grow (decay) at rate λ_1, which is bound to numerically overflow (underflow). To overcome this numerical instability, the QR algorithm executes periodic orthonormalisations of $\boldsymbol{M}$. By denoting the time step with a superscript, the calculation of the Lyapunov exponents and covariant Lyapunov vectors is enabled by the following algorithm.

1. Set the initial condition $\bar{\mathbf{x}}^0$ and initialise $\boldsymbol{M}^0$ to a random orthonormal set of vectors $[\boldsymbol{g}_1 \dots \boldsymbol{g}_m]$.
2. Evolve $\bar{\mathbf{x}}^0, \boldsymbol{M}^0$ using (1), (6) for n_{su} iterations, where n_{su} is called the spinup time, which must be sufficiently large such that $\bar{\mathbf{x}}^{n_{su}}$ is in the attractor (to some numerical tolerance).

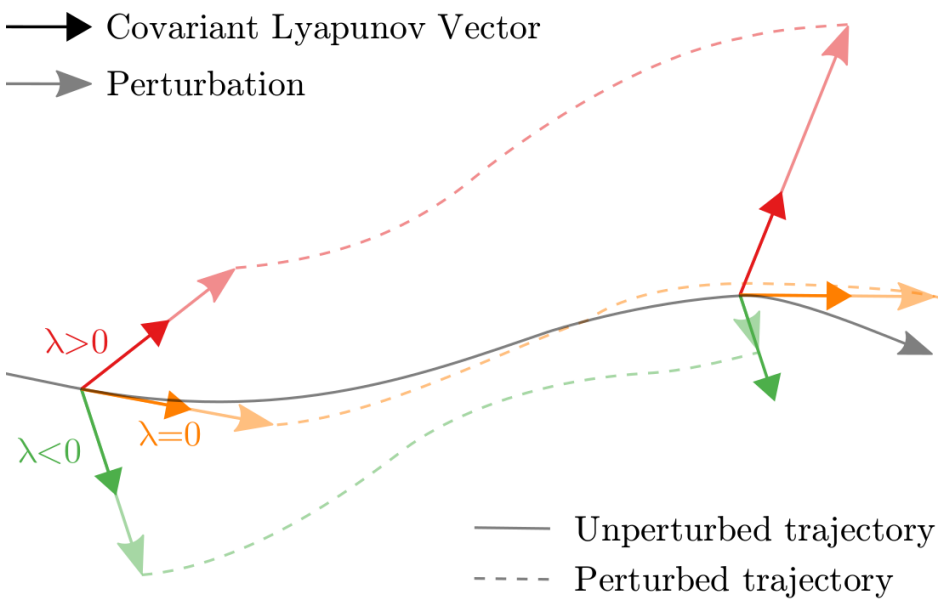

Figure 3: Schematic diagram of covariant Lyapunov vectors and perturbations on an unperturbed trajectory (solid grey line). Three covariant Lyapunov vectors are shown at two different instants, each associated with a different Lyapunov exponent, which can be positive, zero or negative. The decay/growth of three perturbations, along the stable (green), neutral (orange), unstable (red) covariant Lyapunov vector, respectively. The resulting perturbed trajectories (dashed lines), converge, remain at a constant distance, or diverge, respectively, to/from the unperturbed trajectory, depending on the sign of the Lyapunov exponent. This explains why trajectories emanating from two very close initial conditions will almost surely diverge in chaotic systems – it is highly unlikely for the vector connecting the two initial conditions not to have a component in the direction of the unstable covariant Lyapunov vector. Adapted from [4].

3. Evolve $\bar{\mathbf{x}}^j, \boldsymbol{M}^j$ for n_{QR} iterations.

4. Perform QR decomposition on $\boldsymbol{M}^j$, obtaining $\mathbf{x}^j, \boldsymbol{R}^j$. Store $\mathbf{x}^j, \boldsymbol{R}^j$, and set $\boldsymbol{M}^j := \mathbf{x}^j$. If $j < n_T$, where n_T is the total number of iterations corresponding to the total simulation time, go back to Item (3).

5. Randomly initialise an upper triangular matrix $\boldsymbol{C}^{n_T}$ of the same dimension as all $\boldsymbol{R}^j$.

6. Evolve $\boldsymbol{C}^j$ backward by solving $\boldsymbol{R}^j\boldsymbol{C}^j = \boldsymbol{C}^{j+1}$ for $\boldsymbol{C}^j$ and subsequently normalise its columns, i.e. ensuring $\sum_k (\boldsymbol{C}^j_{lk})^2 = 1$.

7. Compute Lyapunov exponents: $[\lambda_1 \dots \lambda_m] = ((n_T - n_{su})\Delta t)^{-1} \sum_{j=n_{su}}^{n_T} \log(|\mathrm{diag}(\boldsymbol{R}^j)|)$, where Δt is the time step.

8. Compute covariant Lyapunov vectors: $[\boldsymbol{\phi}_1|\dots|\boldsymbol{\phi}_m]^j = \mathbf{x}^j\boldsymbol{C}^j$, valid only for $j \in [n_{su}, n_T - n_{sd}]$, where n_{sd} is the spindown time, which must be sufficiently large for $\boldsymbol{C}^j$ to converge to the covariant Lyapunov vector expansion coefficients.

3.3 Non-intrusive computation of the dominant Lyapunov exponent and covariant Lyapunov vector

In this subsection, we focus on the dominant Lyapunov exponent and covariant Lyapunov vector. The adjective "dominant" will be dropped for brevity unless necessary for clarity. Moreover, the dominant Lyapunov exponent will be denoted λ, i.e., the subscript 1 is dropped. Obtaining accurate estimates of the Lyapunov exponent and covariant Lyapunov vector is straightforward even in large-scale simulations. A non-intrusive method is based on the calculation of the *separation* trajectory, also known as the *error*

trajectory. The separation trajectory is the difference between two nearby trajectories (which can be Eulerian fields), which originate from two close initial conditions. Because it is almost sure for the separation trajectory to have a component–even miniscule–in the direction of the dominant covariant Lyapunov vector, the separation trajectory will almost surely diverge along the covariant vector with an exponential divergence rate provided by the Lyapunov exponent. This is why the (dominant) Lyapunov exponent and (dominant) covariant Lyapunov vector are of paramount importance in chaotic flows. They can be calculated as described in the following practical and non-intrusive algorithm.

1. **Statistically converged solution.** Run a numerical simulation (1) until statistical convergence is reached ($\bar{\mathbf{x}}(t)$).

2. **Reset time**, $t = t_0$.

3. **Perturb**. At $t = t_0$, evaluate the perturbed solution $\mathbf{x}^*$ as

$$\mathbf{x}^*(t_0) = \bar{\mathbf{x}}(t_0) + \epsilon||\bar{\mathbf{x}}(t_0)||, \tag{20}$$

   where ϵ is a small number, typically in the range $10^{-9} - 10^{-3}$ and $||\mathbf{x}(t_0)||$ is a norm of order 1.

4. **Separation trajectory.** Advance both solutions, $\bar{\mathbf{x}}(t_0)$ and $\mathbf{x}^*(t_0)$, to some time t_f and evaluate the separation trajectory

$$\Delta\mathbf{x}(t) = \mathbf{x}^*(t) - \bar{\mathbf{x}}(t) \qquad t_0 \leq t \leq t_f. \tag{21}$$

5. **Identification of the linear region** $t_1 \leq t \leq t_2$ where $\ln(\|\Delta\mathbf{x}(t)\|)$ grows linearly. t_f in item 4 must be larger than t_2. If the linear region of the separation trajectory looks noisy, i.e., the local Lyapunov exponent markedly fluctuates, an ensemble simulation is recommended.

6. **Covariant Lyapunov vector.** This is the separation trajectory in the linear region, i.e., $\Delta\mathbf{x}(t)$ $t_1 \leq t \leq t_2$.

7. **Lyapunov exponent.** The Lyapunov exponent is the slope of the linear region, which can be obtained by linear regression

$$\lambda = \frac{1}{t_2 - t_1} \ln\left(\frac{\|\Delta\mathbf{x}(t_2)\|}{\|\Delta\mathbf{x}(t_1)\|}\right). \tag{22}$$

3.4 Predictability

Several definitions of predictability are offered in the literature [12]. However, for the purpose of this chapter, the *predictability* is defined as the *Lyapunov time*, which is the inverse of the Lyapunov exponent

$$t_p \equiv \frac{1}{\lambda}. \tag{23}$$

From Eq.(22), the predictability is the time that a norm of the separation trajectory takes to get amplified by $e \approx 2.718$. Physically, the predictability provides a time scale for the divergence of two nearby trajectory due to the chaotic nature of turbulent flows. In turbulent (reacting and non-reacting) large-eddy and direct numerical simulations, as the grid resolution approaches the smallest physical scales, the Lyapunov exponent, hence predictability, reaches a plateau [15]. Therefore, the Lyapunov exponent was proposed as a metric to assess the quality of a large-eddy simulation [15]: If grid a has the same Lyapunov exponent as grid b, the grid with fewer degrees of freedom can be used to predict rare and transient deterministic events.

3.5 Example: Mathematical connection between eigenvalue analysis and covariant Lyapunov vector analysis on fixed points

Covariant Lyapunov vector analysis is the most general linear stability tool because it can be applied to aperiodic solutions (§3.1). When covariant Lyapunov vector analysis is applied to a fixed point, we recover eigenvalue analysis. Eigenvalue analysis determines the linear stability of a fixed point of $\boldsymbol{F}$. Mathematically, in decomposition (2), $\bar{\mathbf{x}}$ does not depend on time. The linearised dynamics around the fixed point $\bar{\mathbf{x}}$ is governed by (3) where the Jacobian $\boldsymbol{J} = d\boldsymbol{F}/d\mathbf{x}|_{\bar{\mathbf{x}}}$ is constant. The formal solution for an initial condition reads

$$\mathbf{x}'(t) = e^{\boldsymbol{J}t}\mathbf{x}'_0. \tag{24}$$

By assuming that $\boldsymbol{J}$ has a complete eigenbasis, i.e. it is not defective, $\mathbf{x}'_0$ can be decomposed in the eigenbasis $\{\hat{\mathbf{x}}_1, \ldots, \hat{\mathbf{x}}_N\}$, where $\hat{()}_j$ is an eigenvector of $\boldsymbol{J}$, as

$$\mathbf{x}'_0 = \sum_{j=1}^{N} \underbrace{(\mathbf{x}'_0 \cdot \hat{\mathbf{x}_j})}_{\equiv \alpha_j} \hat{\mathbf{x}}_j, \tag{25}$$

where, to keep a similar notation to covariant Lyapunov vector analysis, the eigenpairs are sorted in descending order according to the real part of the corresponding eigenvalue σ_j, i.e. $j = 1$ denotes the eigenpair with largest growth rate. Substituting (25) in (24) yields

$$\begin{aligned}\mathbf{x}'(t) &= e^{\boldsymbol{J}t} \sum_{j=1}^{N} \alpha_j \hat{\mathbf{x}}_j \\ &= \sum_{j=1}^{N} \alpha_j e^{\sigma_j t} \hat{\mathbf{x}}_j.\end{aligned} \tag{26}$$

Substituting the perturbation (26) into the definition of Lyapunov exponent, (8), yields

$$\begin{aligned}\lambda &= \lim_{t\to\infty} \frac{1}{t} \log \frac{\left|\left|\sum_{j=1}^{N} \alpha_j e^{\sigma_j t} \hat{\mathbf{x}}_j\right|\right|}{||\mathbf{x}'_0||} \\ &= \lim_{t\to\infty} \frac{1}{t} \log \left(\frac{|e^{\sigma_k t}|\, ||\alpha_k \hat{\mathbf{x}}_k||}{||\mathbf{x}'_0||} \right) \\ &= \lim_{t\to\infty} \frac{1}{t} \left[\log \left(e^{\mathcal{R}(\sigma_k)t} \right) + \log \left(\frac{||\alpha_k \hat{\mathbf{x}}_k||}{||\mathbf{x}'_0||} \right) \right] \\ &= \mathcal{R}(\sigma_k),\end{aligned} \tag{27}$$

where k is the first index such that $\alpha_k \neq 0$, and $\mathcal{R}$ denotes the real part. Equation (27) shows that the k-th Lyapunov exponent, λ_k, of a linear system on a fixed point is the real part of the eigenvalue of the Jacobian, $\mathcal{R}(\sigma_k)$. Physically, the Lyapunov exponent is the growth (or decay) rate of small perturbations on top of the steady solution. This means that the Lyapunov exponent associated with the perturbation $\mathbf{x}'_0$ is $\mathcal{R}(\sigma_k)$ if $\mathbf{x}'_0$ does not belong to $\mathrm{Span}(\hat{\mathbf{x}}_1, \ldots, \hat{\mathbf{x}}_{k-1})$, which is the subspace spanned by the first $k-1$ eigenvectors.

3.5.1 Exercise: Equivalence between eigenvectors and covariant Lyapunov vectors on fixed points

3.6 Exercise: Mathematical connection between Floquet and covariant Lyapunov vector analysis in periodic solutions.

Show that if the attractor is a limit cycle, the Lyapunov exponents correspond to the real part of the Floquet exponents and that the covariant Lyapunov vectors correspond to the eigenvectors of the monodromy matrix. Hint: Consider the tangent problem (3). We assume that the solution is a limit cycle, i.e. the solution is T-periodic, i.e. $\bar{\mathbf{x}}(t+T) = \bar{\mathbf{x}}(t)$, hence, the Jacobian is T-periodic, i.e. $\boldsymbol{J} \equiv d\boldsymbol{F}/d\mathbf{x}|_{\bar{\mathbf{x}}(t)}$. Let $\boldsymbol{Q}(t) = [\boldsymbol{Q}_1|\dots|\boldsymbol{Q}_N]$ be the fundamental matrix and $\boldsymbol{B}$ the monodromy matrix [24], i.e.

$$\mathbf{x}'(t) = \boldsymbol{Q}(t)\boldsymbol{c}, \tag{28}$$

$$\boldsymbol{Q}(t+T) = \boldsymbol{Q}(t)\boldsymbol{B}, \tag{29}$$

where $\boldsymbol{c}$ is the initial condition, $\mathbf{x}'(0)$, in the basis $\{\mathbf{x}_1(0), \dots, \mathbf{x}_N(0)\}$. Let $\boldsymbol{b}_j$ be the eigenvector of $\boldsymbol{B}$ corresponding to the Floquet multiplier $\rho_j = e^{\nu_j T}$, where ν_j is the j-th Floquet exponent, sorted in descending order according to its real part, i.e. $j = 1$ denotes the Floquet exponent with largest growth rate.

Although the mathematics is more involved, the connection between Floquet analysis and covariant Lyapunov vector analysis naturally follows the connection with eigenvalue analysis of fixed points: a limit cycle can be viewed as a fixed point of a Poincaré map.

3.7 A prototypical chaotic system: The Lorenz system

The Lorenz system (30) is a deterministic nonlinear ordinary differential system, with three positive parameters σ, ρ, β:

$$\begin{cases} \frac{dx}{dt} &= \sigma(y-x) \\ \frac{dy}{dt} &= x(\rho-z)-y \\ \frac{dz}{dt} &= xy-\beta z \end{cases} \tag{30}$$

For certain values of these parameters, the most common and used originally by Lorenz himself being $\sigma = 10$, $\beta = 8/3$ and $\rho = 28$, the system has chaotic solutions. Given the relative simplicity of the equations, low dimensionality of the system and the vast amount of research available on it, the Lorenz system is a prime candidate for getting started with chaotic theory.

3.8 Fixed point analysis

Denoting the state vector $\mathbf{x} = (x, y, z)^T$, the system can be rewritten as $\dot{\mathbf{x}} = \boldsymbol{F}(\mathbf{x})$. The fixed points of the system are determined by solving $\dot{\mathbf{x}} = 0 \rightarrow \boldsymbol{F}(\mathbf{x}) = 0$, which, apart from the trivial fixed point $\mathbf{x}^* = 0$, yields:

$$\begin{cases} x^* = y^* &= \pm\sqrt{\beta(\rho-1)} \\ z^* &= \rho - 1 \end{cases} \tag{31}$$

Therefore, for $\rho \leq 1$, only the trivial fixed point $\mathbf{x}^* = 0$ exists. At $\rho = 1$, the system undergoes a pitchfork bifurcation, after which two new families of fixed points appear $\mathcal{C}^-$, $\mathcal{C}^+$. The linear stability of these can be determined by analysing the Jacobian matrix of the system (32).

$$\boldsymbol{J} \equiv \left.\frac{d\boldsymbol{F}}{d\mathbf{x}}\right|_{\mathbf{x}=\mathbf{x}^*} = \begin{pmatrix} -\sigma & \sigma & 0 \\ \rho - z^* & -1 & -x^* \\ y^* & x^* & -\beta \end{pmatrix} \tag{32}$$

For the trivial fixed point, $\mathbf{x}^* = 0$, the equation in z becomes decoupled and the eigenvalues are easily determined:

$$\lambda_1 = -\beta, \quad \lambda_{2,3} = \frac{-(\sigma+1) \pm \sqrt{(\sigma+1)^2 + 4\sigma(\rho-1)}}{2}$$

The origin is therefore linearly stable for $\rho < 1$ and linearly unstable for $\rho > 1$.
For $\mathcal{C}^\pm$, the characteristic polynomial of J is a third-degree polynomial given in (33).

$$p(\lambda) \equiv \det(J - \lambda\mathcal{I}) = -\lambda^3 - \lambda^2(\beta+\sigma+1) - \lambda\beta(\sigma+\rho) - 2\beta\sigma(\rho-1) \tag{33}$$

Instead of trying to solve a third-degree polynomial equation $p(\lambda) = 0$ directly, one can look for a Hopf bifurcation, where a complex conjugate pair crosses the imaginary axis, by setting $\lambda = i\mu$ with $\mu \in \mathbb{R}$. This results in two equations: one for the real and one for the imaginary part. By solving each one for μ and equating the results, the stability condition (34) is obtained.

$$\rho < \sigma\frac{\sigma+\beta+3}{\sigma-\beta-1} \tag{34}$$

With the classic parameter values $\sigma = 10$, $\beta = 8/3$ and $\rho = 28$, all three fixed points are unstable.

3.9 Strange attractor

With the classic parameter values $\sigma = 10$, $\beta = 8/3$ and $\rho = 28$, the trajectories will converge towards the Lorenz attractor. Figures 4 show three-dimensional, x-y and x-z views of the trajectory with initial condition $\mathbf{x}_0 = (10^{-9}, 10^{-9}, 10^{-9})^T$ up to $t = 50$.

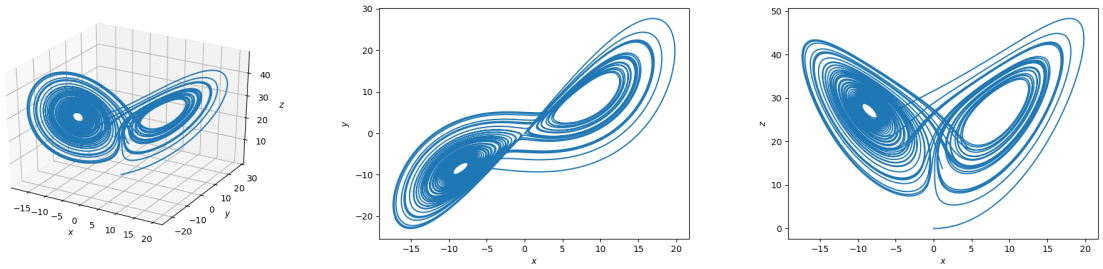

Figure 4: Strange attractor in the Lorenz system.

3.10 Largest Lyapunov exponent

Figure 5 is a graph of the exponential growth of the separation trajectory, $\delta\mathbf{x}$, between the trajectory starting at $\mathbf{x}_0 = (-8.67139571762, 4.98065219709, 25.0)^T$ and at $\mathbf{x}_0 + \delta\mathbf{x}_0$, with $\delta\mathbf{x}_0 = (0, 0, 10^{-9})^T$. It shows that $\log||\frac{\delta\mathbf{x}(t)}{\delta\mathbf{x}_0}||$ starts at 0, follows a linear growth until $t = 25$, finally reaching a plateau. The largest Lyapunov exponent is calculated by a linear regression applied in $t \in [0, 25]$ and its value is $\lambda_1 = 0.929$. To obtain a better estimate, the calculated value of λ_1 should be averaged over many simulations.

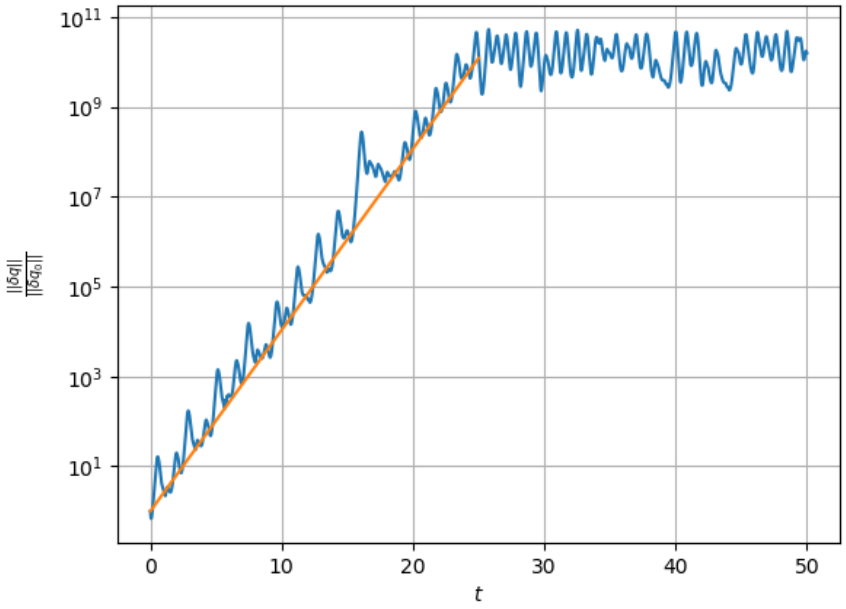

Figure 5: Separation trajectory in the Lorenz system. The dominant Lyapunov exponent is $\lambda \approx 0.929$, which is obtained by linear regression.

3.11 Exercise: Lyapunov spectrum and covariant basis.

The method utilised in the previous section is simple because it requires only the nonlinear code, but it can only determine the largest Lyapunov exponent. Calculate the Lyapunov spectrum of the chaotic solution.

1. Calculate the sum of the Lyapunov exponents.

2. What is meaning of the sum of the Lyapunov exponents?

3. Comment on the convergence of the Lyapunov exponents.

4 Sensitivity analysis

Parts of this section are adapted from [25].

4.1 Sensitivity of time-averaged cost functionals

We wish to optimize the time average of a cost functional, $\mathcal{J} : \mathbb{R}^N \times \mathbb{R}^M \to \mathbb{R}$, of a fluid system

$$\langle \mathcal{J} \rangle \equiv \lim_{T\to\infty} \mathcal{J}_T = \lim_{T\to\infty} T^{-1} \int_0^T \mathcal{J} dt. \tag{35}$$

Examples are the emissions of an aeronautical combustor, drag of a wing/aerofoil, acoustic energy of a combustor, etc. The objective is to calculate the sensitivity (i.e., the gradient) of a cost functional with respect to parameters that can be changed by engineers. The gradient is then embedded in an optimization routine to find the set of parameters that minimize/maximize the cost functional.
We perturb the parameters of the problem (1) as $\mathbf{p} \to \mathbf{p} + \delta\mathbf{p} \implies \mathbf{x} \to \mathbf{x} + \delta\mathbf{x}$ with $\delta(\cdot)$ denoting the infinitesimal perturbation of $(\cdot)$. Hence, the evolution equation is an inhomogeneous tangent equation

$$\frac{d\delta\mathbf{x}}{dt} = \frac{\partial \boldsymbol{F}}{\partial \mathbf{x}}\delta\mathbf{x} + \frac{\partial \boldsymbol{F}}{\partial \mathbf{p}}\delta\mathbf{p} \tag{36}$$

$$\delta\mathbf{x}(t_0) = 0. \tag{37}$$

Note that the initial condition is homogeneous because the source term $\partial\boldsymbol{F}/\partial\mathbf{p}$ works as an impulsive initial condition at $t = t_0$. We wish to evaluate the sensitivity of the cost functional with respect to perturbations to the system's parameter $\mathbf{p}$

$$\frac{d\mathcal{J}_T}{d\mathbf{p}} = \tag{38}$$

$$= \frac{1}{T}\frac{d}{d\mathbf{p}}\left(\int_0^T \mathcal{J} dt\right) = \frac{1}{T}\int_0^T \frac{d\mathcal{J}}{d\mathbf{p}} dt \tag{39}$$

$$= \frac{1}{T}\int_0^T \left(\frac{\partial \mathcal{J}}{\partial \mathbf{p}} + \frac{\partial \mathcal{J}}{\partial \mathbf{x}}\frac{d\mathbf{x}}{d\mathbf{p}}\right) dt \tag{40}$$

If the number of parameters s is greater than the number of cost functionals of interest, we use adjoint equations to evaluate the sensitivity of the cost functional.

4.2 Why traditional sensitivity breaks down in chaotic systems

Aerospace fluid systems are unsteady and often chaotic. Examples of chaotic fluids are turbulent fluids, which are pervasive in engineering and computed by Direct Numerical Simulation (DNS), Large-Eddy Simulation (LES) and Detached-Eddy Simulation (DES). Traditional methods to calculate the gradient of $\langle \mathcal{J} \rangle$ with respect to design parameters break down in chaotic flows. This is because chaotic systems are extremely sensitive to perturbations (butterfly effect, Lorenz 1972). Small perturbations to the initial conditions exponentially increase, which results in completely different instantaneous solutions. However, we assume that the statistical quantities do not change with the initial conditions. In other words, we assume ergodicity, which implies that ensemble average is equal to time average. This means that the system's behaviour for time tending to infinity does not depend on initial conditions for almost every initial condition.
It is convenient, though not necessary, to define the sensitivity variable

$$\delta\mathbf{x}_\mathbf{p} \equiv \frac{d\mathbf{x}}{d\mathbf{p}} \tag{41}$$

such that the sensitivity tangent equation reads

$$\frac{d\delta\mathbf{x_p}}{dt} = \frac{\partial \boldsymbol{F}}{\partial \mathbf{x}}\delta\mathbf{x_p} + \frac{\partial \boldsymbol{F}}{\partial \mathbf{p}} \tag{42}$$

$$\delta\mathbf{x_p}(t_0) = 0. \tag{43}$$

t_0 is set to zero without loss generality. The solution of the tangent system (42) is

$$\delta\mathbf{x_p} = \delta\mathbf{x}_{\mathbf{p},H} + \delta\mathbf{x}_{\mathbf{p},P} \tag{44}$$

where H stands for homogeneous and P stands for particular. These solutions read, respectively

$$\delta\mathbf{x}_{\mathbf{p},H} = \mathcal{P}\left(\exp\left(\int_0^t \frac{\partial \boldsymbol{F}}{\partial \mathbf{x}} d\tilde{t}\right)\right)\delta\mathbf{x}_{\mathbf{p},0} \tag{45}$$

$$\delta\mathbf{x}_{\mathbf{p},P} = \int_0^t \mathcal{P}\left(\exp\left(\int_{\tilde{t}}^t \frac{\partial \boldsymbol{F}}{\partial \mathbf{x}} dt^*\right)\right)\frac{\partial \boldsymbol{F}}{\partial \mathbf{p}} d\tilde{t} \tag{46}$$

We decompose the perturbation onto the complete basis provided by the covariant Lyapunov vectors

$$\delta\mathbf{x}_{\mathbf{p},0} = \sum_{i=0}^{N} c_i \boldsymbol{\phi}(0) \tag{47}$$

$$\frac{\partial \boldsymbol{F}}{\partial \mathbf{p}} = \sum_{i=0}^{N} k_i \boldsymbol{\phi}(\tilde{t}) \tag{48}$$

where N is the dimension of the finite-dimensional space, c_i and k_i are the projections of the quantities on the left-hand side onto the CLVs, $\boldsymbol{\phi}_i(t)$. The first equation is zero because we imposed homogeneous initial conditions, $\delta\mathbf{x_p}(0) = 0$. However, the second equation is not zero for $t = 0$. Therefore, any component in the unstable subspace will tend to grow with the maximal Lyapunov exponent, and $\delta\mathbf{x_p}$ will align with the corresponding CLV. The same reasoning can be applied to the adjoint equation by considering the adjoint CLVs. All in all, the forward (or adjoint) sensitivities

$$\frac{1}{T}\int_0^T \left(\frac{\partial \mathcal{J}}{\partial \mathbf{x}}\right)^T \delta\mathbf{x}_s dt = \int_0^T \left(\frac{\partial \boldsymbol{F}}{\partial s}\right)^T \delta\mathbf{x}_s^+ dt \tag{49}$$

will grow exponentially in time (or in reversed time) with a growth rate provided by the largest Lyapunov exponent. This is the breakdown of traditional sensitivity analysis in chaotic systems, which, in other words, means that in a chaotic system derivatives generally do not commute with the limit

$$\frac{d}{d\mathbf{p}}\langle\mathcal{J}\rangle_\infty \neq \left\langle\frac{d\mathcal{J}}{d\mathbf{p}}\right\rangle_\infty. \tag{50}$$

4.2.1 Exercise: Calculate the sensitivity of the expectation by finite difference

Consider the uniform probability distribution in the interval $[0, 1+\epsilon]$ where $\epsilon \to 0$.

1. What is the expectation?
2. What is the sensitivity of the expectation to ϵ?
3. Compute numerically the sensitivity by finite difference starting with $\epsilon = 10^{-6}$ and 10^6 samples. Discuss the results by varying ϵ and the number of samples.

4.2.2 Sensitivity in ergodic hyperbolic attractors

Shadowing-based sensitivity methods integrate the sensitivity of the cost functional along the shadow trajectory, which does not diverge from the attractor. This way, the quantity sensitivity is bounded. Shadowing-based sensitivity methods [26] are centred around the shadowing lemma [27]. Intuitively, the shadowing lemma guarantees, under some strong assumptions[1] [27], that even in chaotic systems where infinitely close trajectories diverge, there is a trajectory of a slightly perturbed system that does not diverge from the unperturbed system. The original shadowing method [26] achieves this by calculating the perturbation to $\boldsymbol{F}$ in (1) due to a perturbation in a parameter $\mathbf{p} \to \mathbf{p} + \delta\mathbf{p}$, that is, $\partial\boldsymbol{F}/\partial\mathbf{p} \cdot \delta\mathbf{p}$. The perturbation is decomposed in the covariant Lyapunov vector basis of the baseline trajectory to obtain a set of independent ordinary differential equations, one for each mode. The solutions of these equations are the components of the shadow trajectory in the covariant Lyapunov vector basis. After obtaining the perturbed trajectory in the phase space, the sensitivities can be computed.

4.3 Adjoint equations

The adjoint equations of a generic nonlinear dynamical system are derived and discussed. Adjoint equations are crucial for variational data assimilation. The dynamical system is governed by a set of ordinary differential equations, which can be cast as

$$\mathbf{F}\left(\mathbf{x}, \dot{\mathbf{x}}, \mathbf{p}, t\right) = 0, \tag{51}$$

$$\mathbf{g}\left(\mathbf{x}(0), \mathbf{p}\right) = 0, \tag{52}$$

where $\mathbf{F}$ is a nonlinear implicit operator that depends on the parameters $\mathbf{p}$, and $\mathbf{g}$ is a nonlinear function that sets the initial conditions. This is a generalization of the nonlinear system (1).
The objective of sensitivity analysis is to calculate the gradient of the quantity of interest, $\mathcal{J}$, with respect to the parameters

$$\boxed{\frac{\mathrm{d}\mathcal{J}(\mathbf{x}, \mathbf{p})}{\mathrm{d}\mathbf{p}} = \frac{\partial\mathcal{J}}{\partial\mathbf{p}} + \frac{\partial\mathcal{J}}{\partial\mathbf{x}}\frac{\mathrm{d}\mathbf{x}}{\mathrm{d}\mathbf{p}}.} \tag{53}$$

A Lagrangian functional is defined

$$\mathcal{L} \equiv \mathcal{J}(\mathbf{x}, \mathbf{p}) - \langle \mathbf{q}^{+}, \mathbf{F}\left(\mathbf{x}, \dot{\mathbf{x}}, \mathbf{p}, t\right)\rangle - \boldsymbol{\mu}^{T}\mathbf{g}(\mathbf{x}(0), \mathbf{p}), \tag{54}$$

where $\mathbf{q}^{+} \in \mathbb{R}^{N}$ and $\boldsymbol{\mu} \in \mathbb{R}^{N}$ are the as-yet-unknown Lagrangian multipliers; $\dot{\mathbf{x}} \equiv \frac{\mathrm{d}\mathbf{x}}{\mathrm{d}t}$; and

$$\langle \mathbf{a}, \mathbf{b}\rangle \equiv \frac{1}{T}\int_{0}^{T} \mathbf{a}^{T}\mathbf{b}\,\mathrm{d}t \tag{55}$$

is an inner product, where $\mathbf{a}$ and $\mathbf{b}$ are arbitrary vectors in $\mathbb{R}^{N}$. Although not necessary (further simplifications follow in the next sections), the cost functional is considered in the form of a time average over $[0, T]$

$$\mathcal{J}(\mathbf{x}, \mathbf{p}) = \frac{1}{T}\int_{0}^{T} \tilde{\mathcal{J}}(\mathbf{x}, \mathbf{p})\mathrm{d}t. \tag{56}$$

Because of the constraints (51)-(52), it follows that

$$\frac{\mathrm{d}\mathcal{L}}{\mathrm{d}\mathbf{p}} = \frac{\mathrm{d}\mathcal{J}}{\mathrm{d}\mathbf{p}}. \tag{57}$$

[1] See appendix B

Therefore, the total derivative of the Lagrangian reads

$$\begin{aligned}\frac{\mathrm{d}\mathcal{L}}{\mathrm{d}\mathbf{p}} = &\frac{1}{T}\int_0^T \left(\frac{\partial\tilde{\mathcal{J}}}{\partial\mathbf{p}} + \frac{\partial\tilde{\mathcal{J}}}{\partial\mathbf{x}}\frac{\mathrm{d}\mathbf{x}}{\mathrm{d}\mathbf{p}}\right)\mathrm{d}t + \\ &-\frac{1}{T}\int_0^T \mathbf{q}^{+T}\left(\frac{\partial\mathbf{F}}{\partial\mathbf{p}} + \frac{\partial\mathbf{F}}{\partial\mathbf{x}}\frac{\mathrm{d}\mathbf{x}}{\mathrm{d}\mathbf{p}} + \frac{\partial\mathbf{F}}{\partial\dot{\mathbf{x}}}\frac{\mathrm{d}\dot{\mathbf{x}}}{\mathrm{d}\mathbf{p}}\right)\mathrm{d}t + \\ &-\boldsymbol{\mu}^T\left(\frac{\partial\mathbf{g}}{\partial\mathbf{p}} + \frac{\partial\mathbf{g}}{\partial\mathbf{x}(0)}\frac{\mathrm{d}\mathbf{x}(0)}{\mathrm{d}\mathbf{p}}\right),\end{aligned} \tag{58}$$

which, after some re-arrangement and integration by parts, reads

$$\begin{aligned}\frac{\mathrm{d}\mathcal{L}}{\mathrm{d}\mathbf{p}} = &\frac{1}{T}\int_0^T \frac{\partial\tilde{\mathcal{J}}}{\partial\mathbf{p}}\mathrm{d}t + \\ &-\frac{1}{T}\int_0^T \Big(-\frac{\partial\tilde{\mathcal{J}}}{\partial\mathbf{x}} + \mathbf{q}^{+T}\frac{\partial\mathbf{F}}{\partial\mathbf{x}} - \\ &\qquad \mathbf{q}^{+T}\frac{\mathrm{d}}{\mathrm{d}t}\left(\frac{\partial\mathbf{F}}{\partial\dot{\mathbf{x}}}\right) - \frac{\mathrm{d}\mathbf{q}^{+T}}{\mathrm{d}t}\frac{\partial\mathbf{F}}{\partial\dot{\mathbf{x}}}\Big)\frac{\mathrm{d}\mathbf{x}}{\mathrm{d}\mathbf{p}}\mathrm{d}t + \\ &-\frac{1}{T}\int_0^T \mathbf{q}^{+T}\frac{\partial\mathbf{F}}{\partial\mathbf{p}}\mathrm{d}t \\ &-\frac{1}{T}\left[\mathbf{q}^{+T}\frac{\partial\mathbf{F}}{\partial\dot{\mathbf{x}}}\frac{\mathrm{d}\mathbf{x}}{\mathrm{d}\mathbf{p}}\right]_0^T - \boldsymbol{\mu}^T\left(\frac{\partial\mathbf{g}}{\partial\mathbf{p}} + \frac{\partial\mathbf{g}}{\partial\mathbf{x}(0)}\frac{\mathrm{d}\mathbf{x}(0)}{\mathrm{d}\mathbf{p}}\right).\end{aligned} \tag{59}$$

The objective is to calculate the gradient information $\frac{\mathrm{d}\mathcal{L}}{\mathrm{d}\mathbf{p}}$ without calculating $\frac{\mathrm{d}\mathbf{x}}{\mathrm{d}\mathbf{p}}$ for any $t \in [0, T]$. By defining the following conditions

$$\mathbf{q}^{+T}(T) = 0, \tag{60}$$

$$\boldsymbol{\mu}^T = \frac{1}{T}\mathbf{q}^{+T}(0)\frac{\partial\mathbf{F}}{\partial\dot{\mathbf{x}}}\Big|_0\left(\frac{\partial\mathbf{g}}{\partial\mathbf{x}(0)}\right)^{-1}, \tag{61}$$

$$\frac{\partial\tilde{\mathcal{J}}}{\partial\mathbf{x}} = \mathbf{q}^{+T}\frac{\partial\mathbf{F}}{\partial\mathbf{x}} - \mathbf{q}^{+T}\frac{\mathrm{d}}{\mathrm{d}t}\left(\frac{\partial\mathbf{F}}{\partial\dot{\mathbf{x}}}\right) - \frac{\mathrm{d}\mathbf{q}^{+T}}{\mathrm{d}t}\frac{\partial\mathbf{F}}{\partial\dot{\mathbf{x}}} \tag{62}$$

the sensitivity of the quantity of interest can be calculated from (59) as

$$\begin{aligned}\frac{\mathrm{d}\mathcal{L}}{\mathrm{d}\mathbf{p}} = \frac{\mathrm{d}\mathcal{J}}{\mathrm{d}\mathbf{p}} = &\frac{1}{T}\int_0^T \left(\frac{\partial\tilde{\mathcal{J}}}{\partial\mathbf{p}} - \mathbf{q}^{+T}\frac{\partial\mathbf{F}}{\partial\mathbf{p}}\right)\mathrm{d}t + \\ &-\frac{1}{T}\mathbf{q}^{+T}(0)\frac{\partial\mathbf{F}}{\partial\dot{\mathbf{x}}}\Big|_0\left(\frac{\partial\mathbf{g}}{\partial\mathbf{x}(0)}\right)^{-1}\frac{\partial\mathbf{g}}{\partial\mathbf{p}}.\end{aligned} \tag{63}$$

4.3.1 Exercise: Simplifications of adjoint equations

In many cases, the nonlinear dynamical system is explicit

$$\mathbf{F}(\mathbf{x}, \dot{\mathbf{x}}, \mathbf{p}, t) = \dot{\mathbf{x}} - \tilde{\mathbf{F}}(\mathbf{x}, \mathbf{p}, t), \tag{64}$$

and initial conditions of the form of

$$\mathbf{g}(\mathbf{x}(0), \mathbf{p}) = \mathbf{x}(0) - \mathbf{x}_0 = 0. \tag{65}$$

1. Derive the adjoint equations.

2. Make the further simplification that the quantity of interest is not an integral quantity, but it is a function evaluated only at the end of a time window, T, i.e. $\mathcal{J} = \mathcal{J}(\mathbf{x}(T), \mathbf{p})$. Derive the adjoint equations.

3. Make the further simplification that the parameters of interest are the initial conditions $\mathbf{p} = \mathbf{x}_0$. Derive the adjoint equations.

4.3.2 More remarks on adjoint equations

- **Labels.** In functional analysis and linear algebra, adjoint operators are also known as dual or back projection operators;

- **Backpropagation in neural networks.** It is another name for adjoint sensitivity with reversed automatic differentiation.

- **Adjoint models are anti-causal.** In the time domain, the adjoint system is anti-causal because it evolves backward in time. This is because the initial condition is prescribed at the end of the integration, $t = T$, i.e. the adjoint variables carry information on the sensitivity of an output to inputs. Adjoint equations are always linear by definition, i.e. they are dual to the tangent equation. They are defined with respect to the Jacobian of the direct system, which, in nonlinear systems, depends on the direct solution (which can be stored or check-pointed to save storage). In the frequency domain, the anti-causality of the adjoint equations results in a modal transformation with opposite sign, i.e. $\mathbf{x} = \hat{\mathbf{x}} \exp(\sigma t)$ and $\mathbf{x}^+ = \hat{\mathbf{x}}^+ \exp(-\sigma^* t)$.

- **Adjoint codes are reverse differentiation codes.** The adjoint code can be regarded as a case of differentiation algorithms in reverse mode. Some example of direct/adjoint algorithms are: Truncation/zero padding, matrix multiplication/conjugate-transpose matrix multiplication, derivative/negative derivative, convolution/cross-correlation;

- **Adjoint solutions are Lagrange multipliers.** In constrained optimization, the adjoint solutions are the Lagrange multipliers of the governing equations in the constrained functional (Eqn. (54)). Thus, the adjoint variables provide the gradient of the quantity of interest, or cost functional, with respect to the variables of the system. The gradient information can be combined with gradient-based optimization algorithms (e.g., steepest descent/ascent, conjugate gradient, etc.);

- **Adjoint models are not physical models per se.** Although adjoint solutions have a physical interpretation as Lagrange multipliers in constrained optimization, adjoint equations can be defined without any cost functional: Only a bilinear form is required (and, of course, the identification of the correct spaces in the continuous approach). When working in complex spaces, instead of a bilinear form a sesquilinear form that defines an inner product is commonly used[2]. Therefore, adjoint equations do depend on the definition of the bilinear/sesquilinear form, which means that an adjoint model is not a physical model per se[3].

- **Adjoint solutions enforce solvability conditions.** In linear algebra, for an inhomogeneous non-invertible linear system to have a solution, the known vector has to be orthogonal to the the solution of the homogeneous adjoint system (solvability condition, or compatibility condition, or Fredholm alternative);

- **Adjoint solutions and Green's functions.** The i-th component of the adjoint solution is the value of the cost functional when the direct solution is the i-th Green's function;

[2]However, self-adjointness can only be defined with an inner product. Some systems may be self-adjoint with respect to an inner product but may not be with respect to other inner products.

[3]This does not imply that no physical information can be extracted from the adjoint model.

- **Testing an adjoint code.** In the time domain, the adjoint system must pass the dot-product test. This test requires the tangent equation, or a finite-difference approximation of it, and checks that at each time step $\mathbf{x}^+(t) \cdot \mathbf{x}(t) =$ constant $\pm$ tol, where tol is a numerical tolerance, as it ought to be[4]. The adjoint code must pass the Taylor test. With respect to a parameter, p_0, that is perturbed as $p_1 = p_0 + \epsilon$

$$\mathcal{J}(p_1) = \mathcal{J}(p_0) + \epsilon \frac{d\mathcal{J}}{dp}\bigg|_{p_0} + O(\epsilon^2), \tag{66}$$

the test is passed if

$$\frac{\mathcal{J}(p_1) - \mathcal{J}(p_0) - \epsilon \frac{d\mathcal{J}}{dp}\Big|_{p_0}}{\epsilon} \sim O(\epsilon), \tag{67}$$

where $\mathcal{J}(p_1)$ is calculated by re-running the code, and $\frac{d\mathcal{J}}{dp}\Big|_{p_0}$ is calculated by the adjoint code. In other words, the left hand side of Eqn. (67), which is the relative error, is a straight line with respect to the perturbation, ϵ.

[4]By (i) projecting the direct equations onto the adjoint function and the adjoint equations onto the direct function, and (ii) combining these two projections; it follows that $d(\mathbf{x}^+(t) \cdot \mathbf{x}(t))/dt = 0$.

5 Variational data assimilation by way of example in thermoacoustics

This section is adapted from [5].

Data assimilation is a method to make a model more predictive given data from external observations. The physical model provides a prediction on the solution, which is called *forecast*, which is *updated* with a statistical learning algorithm to provide a more accurate state, which is called *analysis*.

Data assimilation is useful to *make a qualitative reduced-order model quantitatively accurate.*

Variational data assimilation is an optimal blending of observations with previous system's state estimates (background) to produce optimal initial conditions. A cost functional is defined to measure (i) the statistical distance between the model output and the measurements from experiments; and (ii) the distance between the model's initial conditions and the background knowledge. Its minimum corresponds to the optimal state, which is computed by Lagrangian optimization with the aid of adjoint equations.

The ingredients of variational data assimilation are (i) a reduced-order model to predict the amplitude of thermoacoustic oscillations, which provides the so-called background state vector $\mathbf{x}^{bg}$ at any time, t (red thick line in Fig. 6); (ii) data from external observations, $\mathbf{y}^i$, which is available from high-fidelity simulations or experiments at times t^i (grey diamonds in Fig. 6); and (iii) an educated guess on the parameters of the system, which originates from past experience. The uncertainties on the background solution and observations are here assumed normal and unbiased. $\mathbf{B}$ and $\mathbf{R}$ are the background and observation covariance matrices, respectively, which need to be prescribed. For simplicity, we assume that $\mathbf{B}$ and $\mathbf{R}$ are diagonal with variances B and R (i.e., errors are statistically independent). A cost functional is defined to measure the statistical distance between the background predictions and the evidence from observations. First, we want the state of the system to be as close as possible to the observations. Second, we do not want the improved solution to be "too far" away from the background solution. This is because we trust that our reduced-order model provides a reasonable solution. Mathematically, these two requirements can be met, respectively, by minimizing the following cost functional

$$J = \underbrace{\frac{1}{2}||\mathbf{x}_0 - \mathbf{x}_0^{bg}||^2_{\mathbf{B}}}_{J_{bg}} + \underbrace{\frac{1}{2}\sum_{i=1}^{N_{obs}} ||\mathbf{M}\mathbf{x}^i - \mathbf{y}^i||^2_{\mathbf{R}}}_{J_{obs}} \qquad \text{over} \quad [0,T], \tag{68}$$

where N_{obs} is the number of observations over the assimilation window $[0,T]$. $\mathbf{M}$ is a linear measurement operator, which maps the state space to the observable space (see Eqs. (72)-(73)). Moreover, $||\mathbf{x}_0 - \mathbf{x}_0^{bg}||^2_{\mathbf{B}} \equiv \left(\mathbf{x}_0 - \mathbf{x}_0^{bg}\right)^{\mathrm{T}} \mathbf{B}^{-1} \left(\mathbf{x}_0 - \mathbf{x}_0^{bg}\right)$. Likewise, $||\mathbf{M}\mathbf{x}^i - \mathbf{y}^i||^2_{\mathbf{R}} \equiv \left(\mathbf{M}\mathbf{x}^i - \mathbf{y}^i\right)^{\mathrm{T}} \mathbf{R}^{-1} \left(\mathbf{M}\mathbf{x}^i - \mathbf{y}^i\right)$.
The objective of state estimation is to improve the prediction of the state, $\mathbf{x}$, over the interval $[0,T]$, by reinitializing the background initial conditions, $\mathbf{x}_0^{bg}$, with optimal initial conditions. These optimal initial conditions are called analysis initial conditions, $\mathbf{x}_0^{analysis}$, which are the minimizers of the cost functional (68). We start from a background knowledge of the model's initial conditions, $\mathbf{x}_0^{bg}$, which is provided by the reduced-order model when data is not assimilated. By integrating the system from $\mathbf{x}_0^{bg}$, we obtain the red trajectory in Fig. 6, $\mathbf{x}^{bg}(t)$. The set of observations is assumed to be distributed over an assimilation window at some time instants. Pictorially, the analysis trajectory corresponds to the green thin line in Fig. 6, which is the minimal statistical distance between the background initial condition (magenta thick arrow) and observations (blue thin arrows). This algorithm is known as 4D-Var in weather forecasting [28]. State estimation enables the adaptive update of reduced-order thermoacoustic models whenever data is available.

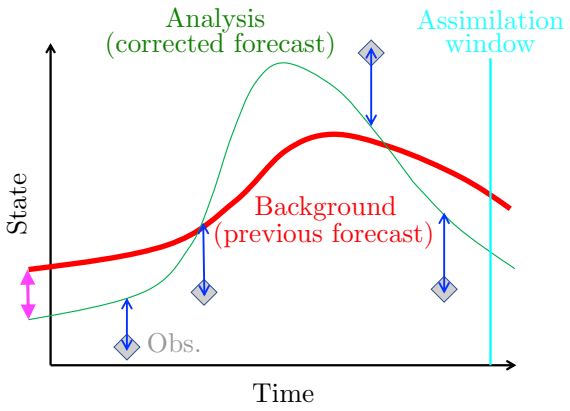

Figure 6: Pictorial representation of variational data assimilation. The background error, J_{bg}, is proportional to the length of the magenta thick arrow, while the observation error, J_{obs}, is proportional to the sum of the blue thin arrows. The vertical cyan line marks the end of the assimilation window, after which the forecast begins. From [5].

5.1 Application to nonlinear thermoacoustic dynamics

When the heat released by a flame is sufficiently in phase with the acoustic pressure, a self-excited thermoacoustic oscillation can arise. These nonlinear oscillations are one of the biggest challenges faced in the design of safe and reliable gas turbines and rocket motors [e.g., 29, 25]. In the worst-case scenario, uncontrolled thermoacoustic oscillations can shake an engine apart. Reduced-order thermoacoustic models, which are nonlinear and time-delayed, can only qualitatively predict thermoacoustic oscillations. To make reduced-order models quantitatively predictive, we can use a data assimilation framework for state estimation.

5.1.1 Nonlinear time-delayed thermoacoustic model

We investigate the acoustics of a resonator excited by a heat source, which is a monopole source of sound. The main assumptions of the reduced-order model are [25]: (i) the acoustics evolve on top of a uniform mean flow; (ii) the mean-flow Mach number is negligible, therefore the acoustics are linear and no flow inhomogeneities are convected; (iii) the flow is isentropic except at the heat-source location; (iv) the length of the duct is sufficiently larger than the diameter, such that the cut-on frequency is high, i.e., only longitudinal acoustics are considered; (v) the heat source is compact, i.e., it excites the acoustics at a specific location, x_f; (vi) the boundary conditions are ideal and open-ended, i.e., the acoustic pressure at the ends is zero. Under these assumptions, the non-dimensional momentum and energy equations are, respectively [30]

$$\frac{\partial u}{\partial t} + \frac{\partial p}{\partial x} = 0, \tag{69}$$

$$\frac{\partial p}{\partial t} + \frac{\partial u}{\partial x} + \zeta p - \dot{\mathcal{Q}}\delta_D(x - x_f) = 0, \tag{70}$$

where u is the acoustic velocity; p is the acoustic pressure; t is the time; x is the axial coordinate of the duct; $\delta_D(x - x_f)$ is the Dirac delta distribution at the heat source location, x_f; ζ is the damping factor, which models the acoustic energy radiation from the boundaries and thermo-viscous losses; and $\dot{\mathcal{Q}}$ is the heat release rate (or, simply, heat release). The heat release, $\dot{\mathcal{Q}}$, may be modelled for our pedagogical purposes by a nonlinear time delayed law [31]

$$\dot{\mathcal{Q}} \equiv \beta \mathrm{Poly}(u_f(t - \tau)), \tag{71}$$

where τ is the time delay; β is the strength of the heat source; and $\mathrm{Poly}(\tilde{u}(\tilde{t})) = a_1\tilde{u}^5(\tilde{t}) + \cdots + a_5\tilde{u}(\tilde{t})$. The time delay and strength of the heat source are the two key parameters of a reduced-order model for

the flame [32]. Physically, τ is the time that the heat release takes to respond to a velocity perturbation at the flame's base; while β provides the strength of the coupling between the heat source and the acoustics. Velocity, pressure, length and time are nondimensionalized as in [30]. The set of nonlinear time-delayed partial differential equations (69)-(70) provides a physics-based reduced-order model for the nonlinear thermoacoustic dynamics. Owing to the assumptions we made, the model can only qualitatively replicate the nonlinear thermoacoustic behaviour. A variational data assimilation method can make a qualitative model quantitatively more accurate any time that reference data can be assimilated. The data can come, for example, from sensors in experiments or time series from high-fidelity simulations.

5.1.2 Numerical discretization with acoustic modes

We use separation of variables to decouple the time and spatial dependencies of the solution. The spatial basis on to which the solution is projected consists of the natural acoustic modes. When decomposed on the natural acoustic eigenfunctions, the acoustic velocity and pressure are, respectively

$$u(x,t) = \sum_{j=1}^{N_m} \eta_j(t)\cos(j\pi x), \tag{72}$$

$$p(x,t) = \sum_{j=1}^{N_m} \left(\frac{\dot{\eta}_j(t)}{j\pi}\right)\sin(j\pi x), \tag{73}$$

where the relationship between η_j and $\dot{\eta}_j$ has yet to be found and N_m is the number of acoustic modes considered. This discretization is sometimes known as the Galerkin discretization [33]. The state of the system is provided by the amplitudes of the Galerkin modes that represent velocity, η_j, and those that represent pressure, $\dot{\eta}_j/(j\pi)$. The damping has modal components, $\zeta_j = C_1 j^2 + C_2\sqrt{j}$, where C_1 and C_2 are damping coefficients [34, 35, 36, 30, 37]. In vector notation, $\boldsymbol{\eta} \equiv (\eta_1, \cdots, \eta_N)^{\mathrm{T}}$ and $\dot{\boldsymbol{\eta}} \equiv (\dot{\eta}_1/\pi, \cdots, \dot{\eta}_N/(N\pi))^{\mathrm{T}}$. The state vector of the discretized system is the column vector $\mathbf{x} \equiv (\boldsymbol{\eta}; \dot{\boldsymbol{\eta}})$. The governing equations of the Galerkin modes are found by substituting (72)-(73) into (69)-(71). Equation (70) is then multiplied by $\sin(k\pi x)$ and integrated over the domain $x = [0, 1]$ (projection). In so doing, the spatial dependency is removed and the Galerkin amplitudes are governed by a set of nonlinear time-delayed differential equations

$$\mathrm{F}_{1j} \equiv \frac{d}{dt}(\eta_j) - j\pi\left(\frac{\dot{\eta}_j}{j\pi}\right) = 0 \qquad t > 0, \tag{74}$$

$$\mathrm{F}_{2j} \equiv \frac{d}{dt}\left(\frac{\dot{\eta}_j}{j\pi}\right) + j\pi\eta_j + \zeta_j\left(\frac{\dot{\eta}_j}{j\pi}\right) = 0 \qquad t \in [0, \tau), \tag{75}$$

$$\mathrm{F}_{2j} \equiv \frac{d}{dt}\left(\frac{\dot{\eta}_j}{j\pi}\right) + j\pi\eta_j + \zeta_j\left(\frac{\dot{\eta}_j}{j\pi}\right) + 2s_j\beta\ \mathrm{Poly}(u_f(t-\tau)) = 0 \qquad t \in [\tau, T], \tag{76}$$

where $u_f(t-\tau) = \sum_{j=1}^{N_m}\eta_j(t-\tau)c_j$; $s_j \equiv \sin(j\pi x_f)$ and $c_j \equiv \cos(j\pi x_f)$. The labels $\mathrm{F}_\bullet$ are introduced for the definition of the Lagrangian (Sec. 5.1.4). Because the Galerkin expansions (72)-(73) are truncated at the N_m-th mode, we obtain a reduced-order model of the original thermoacoustic system (69)-(70) with $2N_m$ degrees of freedom (74)-(76). The reduced-order model is physically a set of $2N_m$ time-delayed oscillators, which are nonlinearly coupled through the heat release term. In the following sections, we employ variational data assimilation to improve the accuracy of such a reduced-order model.

5.1.3 Thermoacoustic cost functionals

Crucial to variational data assimilation is the definition of the cost functionals J_{bg} and J_{obs}. Two physical thermoacoustic cost functionals are proposed and compared to reproduce different scenarios. For the

background error

$$J^a_{bg} = \frac{1}{2B}\left(p(0) - p(0)_{bg}\right)^2 \ , \tag{77}$$

$$J^b_{bg} = \frac{1}{2B}\sum_{j=1}^{N_m}\left\{\left[\left(\frac{\dot{\eta}_{j0}}{j\pi}\right) - \left(\frac{\dot{\eta}_{j0}}{j\pi}\right)_{bg}\right]\sin(j\pi x_m)\right\}^2, \tag{78}$$

$$\tag{79}$$

For the observation error

$$J^a_{obs} = \sum_{i=1}^{N_{obs}} J^a_{obs,i} = \frac{1}{2R}\sum_{i=1}^{N_{obs}}\left(p(t^i_{obs}) - p^{(i)}_{obs}\right)^2, \tag{80}$$

$$J^b_{obs} = \sum_{i=1}^{N_{obs}} J^b_{obs,i} = \frac{1}{2R}\sum_{i=1}^{N_{obs}}\sum_{j=1}^{N_m}\left\{\left[\left(\frac{\dot{\eta}_j(t^i_{obs})}{j\pi}\right) - \left(\frac{\dot{\eta}_j}{j\pi}\right)^{(i)}_{obs}\right]\sin(j\pi x_m)\right\}^2, \tag{81}$$

where x_m is the location where the measurement is taken and t^i_{obs} is the instant at which the $i-$th observation is assimilated. On the one hand, by using J^a_{bg} and J^a_{obs} the analysis solution is optimized against the background pressure at $t = 0$ and the measured pressure at $t = t^i_{obs}$, $i = 1, \ldots, N_{obs}$. Physically, this means that the acoustic pressure is the model output, $p(0)_{bg}$, and the observable from the sensors, p^i_{obs}. On the other hand, J^b_{bg} and J^b_{obs} constrain the pressure modes. Physically, this means that every pressure mode provided by the background solution is a model output, $(\dot{\eta}_{j0}/(j\pi))_{bg}$, and it is assumed that the modes of the acoustic pressure,$(\dot{\eta}_j/(j\pi))^{(i)}_{obs}$, can be calculated from the sensors on the fly.

5.1.4 Lagrangian of the thermoacoustic system

To attain a minimum of J, a necessary condition is that the gradient vanishes, i.e.,

$$\nabla_{\mathbf{x}_0}(J) = \nabla_{\mathbf{x}_0}(J_{bg}) + \sum_{i=1}^{N_{obs}} \nabla_{\mathbf{x}_0}(J_{obs,i}) = 0, \tag{82}$$

where $\nabla_{\mathbf{x}_0}$ is the gradient with respect to the initial conditions. There exists $\mathbf{x}_0$ such that $\nabla_{\mathbf{x}_0}(J) = 0$ because of the convexity of the cost functionals in the neighbourhood of a local extremum. To compute $\nabla_{\mathbf{x}_0}(J_{bg})$ and $\nabla_{\mathbf{x}_0}(J_{obs,i})$, we use calculus of variation (Sec. 5.1.4). The Lagrange multipliers, also known as adjoint, or dual, or co-state variables (Sec. 5.1.5), provide the gradient information with respect to the initial state. The governing equations and their initial conditions are rewritten in the form of constraints, F, which hold over time intervals, while G are the constraints that hold for a specific time only, i.e., $t = t_0$. Together with equations (74)-(76) and by defining the auxiliary variable $\bar{\eta}(t) \equiv u_f(t - \tau)$, they are

$$\mathrm{F}_3 \ \equiv \bar{\eta}(t) = 0, \qquad t \in [0, \tau) \tag{83}$$

$$\mathrm{F}_3 \ \equiv \bar{\eta}(t) - u_f(t - \tau) = 0, \qquad t \in [\tau, T]. \tag{84}$$

The constraints for the initial conditions are

$$\mathrm{G}_{1j} \equiv \eta_j(0) - \eta_{j0} = 0, \tag{85}$$

$$\mathrm{G}_{2j} \equiv \left(\frac{\dot{\eta}_j(0)}{j\pi}\right) - \left(\frac{\dot{\eta}_{j0}}{j\pi}\right) = 0. \tag{86}$$

By defining an inner product

$$[a, b] = \frac{1}{T}\int_0^T ab \ dt \tag{87}$$

where a and b are arbitrary functions. The Lagrangian of the nonlinear system can be written as

$$\mathcal{L} \equiv J_{bg} + J_{obs,i} + \sum_{j=1}^{N_m} \mathcal{L}_j - \left[\bar{\xi}(t), \mathrm{F}_3\right], \tag{88}$$

where each $\mathcal{L}_j$ is

$$\mathcal{L}_j \equiv -\left[\frac{\xi_j}{j\pi}, \mathrm{F}_{1j}\right] - \left[\nu_j, \mathrm{F}_{2j}\right] - b_{1j}\mathrm{G}_{1j} - b_{2j}\mathrm{G}_{2j}, \tag{89}$$

where $\bar{\xi}$, $\xi_j/j\pi$, ν_j and $b_{\bullet j}$ are the Lagrange multipliers, or adjoint variables, of the corresponding constraints. Because we wish to derive the adjoint equations for the cost functional $J_{obs,i}$, we consider the time window to be $T = t^i_{obs}$.

5.1.5 Adjoint equations

First, the Lagrangian (88) is integrated by parts to make the dependence on the direct variables explicit. Secondly, the first variation is calculated by a Fréchet derivative

$$\left[\frac{\partial \mathcal{L}}{\partial \mathbf{x}}, \delta\mathbf{x}\right] \equiv \lim_{\epsilon \to 0} \frac{\mathcal{L}(\mathbf{x} + \epsilon\delta\mathbf{x}) - \mathcal{L}(\mathbf{x})}{\epsilon}. \tag{90}$$

Thirdly, the derivatives of (88) are taken with respect to the initial condition of each variable of the system, $\partial\mathcal{L}/\partial\mathbf{x}_0$. These expressions will be used later to compute the gradient. Finally, to find the set of Lagrange multipliers that characterizes an extremum of the Lagrangian, $\mathcal{L}$, variations with respect to $\delta\mathbf{x}$ are set to zero. The adjoint equations and their initial conditions are derived by setting variations of $\delta\eta_j$, $\delta\left(\dot{\eta}_j/(j\pi)\right)$ and $\delta\bar{\eta}$ to zero over $[0, T]$.
By noting that

$$\left[\bar{\xi}(t), \mathrm{F}_3\right] = \left[\bar{\xi}(t), \bar{\eta}(t)\right]_{t^*}^{T} - \left[\bar{\xi}(t+\tau), u_f(t)\right]_{t^*-\tau}^{T-\tau}, \tag{91}$$

the Lagrangian (88) is integrated by parts to make the dependence on the direct variables explicit, yielding

$$\begin{aligned}
\mathcal{L} = {} & J_{bg} + J_{obs,i} \\
& - \sum_{j=1}^{N_{mod}} \left\{ -\left[\frac{d}{dt}\left(\frac{\xi_j}{j\pi}\right), \eta_j\right] - \left[j\pi\frac{\xi_j}{j\pi}, \frac{\dot{\eta}_j}{j\pi}\right] + \frac{1}{T}\left(\frac{\xi_j(T)}{j\pi}\eta_j(T) - \frac{\xi_j(0)}{j\pi}\eta_j(0)\right) \right\} \\
& - \sum_{j=1}^{N_{mod}} \left\{ -\left[\frac{d\nu_j}{dt}, \frac{\dot{\eta}_j}{j\pi}\right] + \left[j\pi\nu_j, \eta_j\right] + \left[\zeta_j\nu_j, \frac{\dot{\eta}_j}{j\pi}\right] + \left[\ \nu_j, 2\beta s_j \mathrm{Poly}(\bar{\eta}(t))\ \right] + \frac{1}{T}\left(\nu_j(T)\frac{\dot{\eta}_j(T)}{j\pi} - \nu_j(0)\frac{\dot{\eta}_j(0)}{j\pi}\right) \right\} \\
& - \left\{ \left[\bar{\xi}(t), \bar{\eta}(t)\right] - \left[\bar{\xi}(t+\tau), u_f(t)\right]_{t^*-\tau}^{T-\tau} \right\}
\end{aligned} \tag{92}$$

5.1.6 Exercise: Derive the adjoint equations

5.1.7 Gradient-based optimization

The optimization loop consists of the following steps:

1) Integrate the system forward from $t = 0$ to $t = T$ from an initial state $\mathbf{x}_0$;

2) Initialize the adjoint variables;

3) Evolve the adjoint variables backward from $t = T$ to $t = 0$;

4) Evaluate the gradient using the adjoint variables at $t = 0$.

Once the gradient is numerically computed, the cost functional can be minimized via a gradient based optimization loop. The conjugate gradient [38] is used to update the cost functional until the condition $\nabla_{\mathbf{x}_0}(J) = 0$ is attained to a relative numerical tolerance of 10^{-4}. By using a gradient based approach, we find a local minimum of J.

5.1.8 Exercise: Twin experiments for data assimilation

Validate the data-assimilation algorithm by twin experiments. Perturb (i) the true state solution, $\mathbf{x}^{true}(t)$, by perturbing the unstable fixed point at the origin of the phase space, and (ii) the background trajectory, $\mathbf{x}^{bg}(t)$, by perturbing each true mode initial condition with a Gaussian error with variance $B = 0.005^2$. The $i-$th observation is produced by adding a Gaussian error with variance $R = 0.005^2$ to $\mathbf{x}^{true}(t^i_{obs})$. The parameters to use are $\beta = 1$, $\tau = 0.02$, $C_1 = 0.05$, $C_2 = 0.01$ and

$$(a_1, a_2, a_3, a_4, a_5) = (-0.012, 0.059, -0.044, -0.108, 0.5) \tag{93}$$

for the heat release term $\dot{\mathcal{Q}}$. The position of the heat source is $x_f = 0.3$ and all the measurements are taken at $x_m = 0.8$.

1. Show how the number of Galerkin modes affects the solution of the system. Compare at least two solutions using $N_m = 3$ and $N_m = 10$.

2. Use 100 observations in the assimilation window of 0.4 time units. Investigate the effects that the cost functionals J^a and J^b have on the analysis solution. Which one is performing better? Explain why.

3. Discuss the effects that the number of observations has on the analysis by using an assimilation window of 2.5 time units. At regime, what is the minimum number of observations that is necessary for the error to decrease?

---

6 Sequential data assimilation

Parts of this section are adapted from [1].

Statistical learning by data assimilation finds the statistically optimal combination of model predictions and observations by combining concepts from control theory, probability theory and dynamic programming. The data assimilation technique used in this study is the ensemble Kalman filter [39, 40]. In the ensemble Kalman filter, a Monte Carlo approach is used to estimate the statistics at every timestep [41], which makes it (i) a computationally efficient technique in terms of storage requirements, (ii) amenable to parallel computing and (iii) non-intrusive. Compared to other data assimilation techniques based on the Kalman filter, e.g., the extended Kalman filter, the ensemble Kalman filter is particularly suitable for highly nonlinear systems [42], such as premixed flames [2, 3] that display strongly nonlinear events, e.g., cusp formation and pinch-off.

Roadmap. Section 6.1 introduces sequential data assimilation from a more intuitive point of view. The keen reader who wishes to delve into a more general point of view is invited to read Section 6.2.

6.1 Introduction to sequential Data Assimilation with estimators

In sequential data assimilation, a discrete time-dependent problem is considered [42]. We assume that the model prediction at each time step is a function of the model prediction at the previous time step only (*Markov chain*). When measurements become available, the appropriate analysis scheme is used to assimilate the data. The question arises as to what the covariance matrix $C^f_{\psi\psi}$ of the model prediction looks like at any given timestep. The Kalman filter and its descendants describe how the covariance matrix $C^f_{\psi\psi}$ of the model prediction evolves in time (Sec. 6.1.2–6.1.4). The Kalman filter essentially assumes normally distributed error terms, and is exact for linear problems. The extended Kalman filter extends the Kalman filter to nonlinear problems by linearizing the time evolution of the covariance matrix $C^f_{\psi\psi}$. The ensemble Kalman filter avoids the linearization by evolving an ensemble instead of time marching the covariance matrix $C^f_{\psi\psi}$.

6.1.1 Finite-Dimensional Analysis Scheme

We start out with a time-independent problem for simplicity. The model prediction ψ^f and the measurement d are represented as

$$\psi^f = \psi^t + p^f \quad , \tag{94}$$

$$d = M\psi^t + \epsilon \quad , \tag{95}$$

where $\psi^f, \psi^t, p^f \in \mathbb{R}^n$, $d, \epsilon \in \mathbb{R}^m$ and $M \in \mathbb{R}^{m\times n}$. The superscript t denotes the true state. The superscript f denotes the model prediction. p^f denotes the error of the model prediction ψ^f relative to the true state ψ^t. d denotes the measurement. ϵ denotes the measurement error. M is a linear measurement operator. n denotes the number of degrees of freedom of the system, and m denotes the number of measurements available at the same time. The error terms are unbiased and uncorrelated:

$$\overline{p^f} = 0 \quad , \quad \overline{\epsilon} = 0 \quad , \quad \overline{p^f \epsilon^T} = 0 \quad . \tag{96}$$

The covariance matrices are given by

$$\overline{p^f \left(p^f\right)^T} = C^f_{\psi\psi} \quad , \quad \overline{\epsilon \left(\epsilon\right)^T} = C_{\epsilon\epsilon} \quad . \tag{97}$$

The cost functional is given by

$$\mathcal{J}[\psi] = \frac{1}{2}\left(\psi - \psi^f\right)^T C_{\psi\psi}^{-1}\left(\psi - \psi^f\right) + \frac{1}{2}\left(d - M\psi\right)^T C_{\epsilon\epsilon}^{-1}\left(d - M\psi\right) \quad . \tag{98}$$

The first variation of the cost functional is given by

$$\delta\mathcal{J} = \left(\psi - \psi^f\right)^T C_{\psi\psi}^{-1}\delta\psi - \left(d - M\psi\right)^T C_{\epsilon\epsilon}^{-1} M\delta\psi \quad . \tag{99}$$

A necessary condition for a local minimum is

$$C_{\psi\psi}^{-1}\left(\psi^a - \psi^f\right) - M^T C_{\epsilon\epsilon}^{-1}\left(d - M\psi^a\right) = 0 \quad , \tag{100}$$

$$\left[C_{\psi\psi}^{-1} + M^T C_{\epsilon\epsilon}^{-1} M\right]\psi^a = C_{\psi\psi}^{-1}\psi^f + M^T C_{\epsilon\epsilon}^{-1} d \quad . \tag{101}$$

This gives

$$\psi^a = \left[C_{\psi\psi}^{-1} + M^T C_{\epsilon\epsilon}^{-1} M\right]^{-1} C_{\psi\psi}^{-1}\psi^f + \left[C_{\psi\psi}^{-1} + M^T C_{\epsilon\epsilon}^{-1} M\right]^{-1} M^T C_{\epsilon\epsilon}^{-1} d \tag{102}$$

$$= \psi^f + \left[C_{\psi\psi}^{-1} + M^T C_{\epsilon\epsilon}^{-1} M\right]^{-1} M^T C_{\epsilon\epsilon}^{-1}\left(d - M\psi^f\right) \tag{103}$$

$$= \psi^f + C_{\psi\psi} M^T \left[C_{\epsilon\epsilon} + M C_{\psi\psi} M^T\right]^{-1}\left(d - M\psi^f\right) \quad , \tag{104}$$

$$C_{\psi\psi}^a = \left[C_{\psi\psi}^{-1} + M^T C_{\epsilon\epsilon}^{-1} M\right]^{-1} \tag{105}$$

$$= C_{\psi\psi} - C_{\psi\psi} M^T \left[C_{\epsilon\epsilon} + M C_{\psi\psi} M^T\right]^{-1} M C_{\psi\psi} \quad . \tag{106}$$

In Eq. (106), the Woodbury formula is used

$$\left(A_{11} - A_{12}A_{22}^{-1}A_{21}\right)^{-1} = A_{11}^{-1} - A_{11}^{-1}A_{12}\left(A_{21}A_{11}^{-1}A_{12} - A_{22}\right)^{-1} A_{21}A_{11}^{-1} \tag{107}$$

The matrix $C_{\psi\psi} M^T \left[C_{\epsilon\epsilon} + M C_{\psi\psi} M^T\right]^{-1}$ is also known as the *Kalman gain*. It appears in Eq. (104) and (106). The Kalman gain does not have to be explicitly computed because it is more efficient to evaluate it from right to left.
The estimator ψ^a may be viewed as an average of the model prediction ψ^f and the measurement d weighted by their respective variances. The variance $C_{\psi\psi}^a$ of the best estimate is less than the variance $C_{\psi\psi}^f$ of the model prediction.

6.1.2 Kalman Filter

We consider a discrete time-dependent problem

$$\psi_k^f = G\psi_{k-1}^a \quad , \tag{108}$$

where the subscript k denotes the timestep. The state ψ is an n-dimensional vector, G is an n-by-n linear propagator. When measurements are available, the analysis scheme is used to assimilate the data (Sec. 6.1.1). Otherwise, ψ_k^a is the same as ψ_k^f. Like ψ^f and ψ^a, G is imperfect. Comparing the true state ψ_k^f with the model prediction based on the true state ψ_{k-1}^t at the previous timestep gives the model error q_{k-1}:

$$\psi_k^t = G\psi_{k-1}^t + q_{k-1} \quad . \tag{109}$$

The error terms p^a_{k-1} and q_{k-1} are assumed to be unbiased and uncorrelated:

$$\overline{p^a_{k-1}} = 0 \quad , \quad \overline{q_{k-1}} = 0 \quad , \quad \overline{q_{k-1}\left(p^a_{k-1}\right)^T} = 0 \quad . \tag{110}$$

The error p^f_k of the model prediction ψ^f_k is given by

$$p^f_k = \psi^f_k - \psi^t_k \tag{111}$$

$$= G\left(\psi^f_{k-1} - \psi^t_{k-1}\right) - q_{k-1} \quad . \tag{112}$$

The covariance matrix $\left(C^f_{\psi\psi}\right)_k$ of the model prediction is given by

$$\left(C^f_{\psi\psi}\right)_k = \overline{\left(\psi^f_k - \psi^t_k\right)\left(\psi^f_k - \psi^t_k\right)^T} \tag{113}$$

$$= G\left(C^f_{\psi\psi}\right)_{k-1} G^T + \overline{q_{k-1}q^T_{k-1}} \quad . \tag{114}$$

Thus, the covariance matrix $C^f_{\psi\psi}$ at a timestep k depends on the covariance matrix $C^f_{\psi\psi}$ at the timestep $k-1$ and the model error q introduced when integrating from $k-1$ to k.

6.1.3 Extended Kalman Filter

If the matrix G is replaced by a nonlinear propagator $G : \mathbb{R}^n \to \mathbb{R}^n$, Eq. (108) and (109) become

$$\psi^f_k = G\left[\psi^a_{k-1}\right] \quad , \tag{115}$$

$$\psi^t_k = G\left[\psi^t_{k-1}\right] + q_{k-1} \quad . \tag{116}$$

The error p^f_k of the model prediction ψ^f_k is given by a first-order approximation:

$$p^f_k = \psi^f_k - \psi^t_k \tag{117}$$

$$\approx \frac{\partial G}{\partial \psi}\left[\psi^f_{k-1} - \psi^t_{k-1}\right] - q_{k-1} \quad . \tag{118}$$

The covariance matrix $\left(C^f_{\psi\psi}\right)_k$ of the model prediction is given by

$$\left(C^f_{\psi\psi}\right)_k = \overline{\left(\psi^f_k - \psi^t_k\right)\left(\psi^f_k - \psi^t_k\right)^T} \tag{119}$$

$$\approx \left(\frac{\partial G}{\partial \psi}\right)\left(C^f_{\psi\psi}\right)_{k-1}\left(\frac{\partial G}{\partial \psi}\right)^T + \overline{q_{k-1}q^T_{k-1}} \quad . \tag{120}$$

For strongly nonlinear problems, like fluid mechanics, a first-order approximation may not be enough.

6.1.4 Ensemble Kalman Filter

The extended Kalman filter suffers from two shortcomings:

1. Throughout the time evolution, the error terms are assumed to be normally distributed. This is not correct because a normal distribution generally becomes non-normal under a nonlinear operation G.

2. The analysis scheme is exact for normally distributed error terms, but it is not exact in general.

The ensemble Kalman filter alleviates the first shortcoming. It is a Markov-Chain Monte-Carlo method. The error distribution is realized by an ensemble. The ensemble size N can be much smaller than the number of degrees of freedom of the system. Until a measurement becomes available, the members of the ensemble independently evolve in time. Hence, higher-order moments are taken into account.
The covariance matrix $C^f_{\psi\psi}$ of the model prediction cannot be reconstructed from the ensemble because the true state ψ^t is unknown. For the analysis scheme, it is replaced by the ensemble covariance matrix $C^{ef}_{\psi\psi}$ of the model prediction, which is instead formed around the ensemble average $\overline{\psi^f}$:

$$C^{ef}_{\psi\psi} = \overline{\left(\psi^f - \overline{\psi^f}\right)\left(\psi^f - \overline{\psi^f}\right)^T} \tag{121}$$

$$\approx \frac{1}{N-1}\sum_{j=1}^{N}\left(\left(\psi^f\right)_j - \overline{\psi^f}\right)\left(\left(\psi^f\right)_j - \overline{\psi^f}\right)^T \quad . \tag{122}$$

where the subscript j enumerates the ensemble members. Note that an unbiased ensemble covariance matrix is formed with $N-1$ instead of N.
An estimator ψ^a is given by

$$\left(\psi^a\right)_i = \left(\psi^f\right)_i + C^{ef}_{\psi\psi}M^T\left[C_{\epsilon\epsilon} + MC^{ef}_{\psi\psi}M^T\right]^{-1}\left(d_i - M\left(\psi^f\right)_i\right) \quad . \tag{123}$$

Note that the measurements d_j in Eq. (123) also form an ensemble, which is necessary for a consistent analysis scheme [42]. Otherwise, the ensemble covariance matrix $C^{ea}_{\psi\psi}$ of the best estimate does not converge to $C^a_{\psi\psi}$ in the limit of infinite ensemble size (Eq. (106)). Thus, the measurement d is artificially perturbed for every ensemble member j according to the covariance matrix $C_{\epsilon\epsilon}$ of the measurement. Another option would be the square-root algorithm, which will be discussed in Sec. 6.1.5.
In Eq. (123), the ensemble Kalman gain $C^{ef}_{\psi\psi}M^T\left[C_{\epsilon\epsilon} + MC^{ef}_{\psi\psi}M^T\right]^{-1}$ may be computed using either the covariance matrix $C_{\epsilon\epsilon}$ of the measurement or the ensemble version $C^e_{\epsilon\epsilon}$:

$$C^e_{\epsilon\epsilon} = \overline{\left(d - M\overline{\psi^f}\right)\left(d - M\overline{\psi^f}\right)^T} \tag{124}$$

$$\approx \frac{1}{N-1}\sum_{j=1}^{N}\left(d_j - M\overline{\psi^f}\right)\left(d_j - M\overline{\psi^f}\right)^T \quad . \tag{125}$$

The difference between $C_{\epsilon\epsilon}$ and $C^e_{\epsilon\epsilon}$ is less significant than the introduction of the ensemble covariance matrix $C^{ef}_{\psi\psi}$ of the model prediction.
The ensemble covariance matrix $C^{ea}_{\psi\psi}$ of the best estimate is given by

$$C^{ea}_{\psi\psi} = \overline{\left(\psi^a - \overline{\psi^a}\right)\left(\psi^a - \overline{\psi^a}\right)^T} \tag{126}$$

$$= C^{ef}_{\psi\psi} - C^{ef}_{\psi\psi}M^T\left[C_{\epsilon\epsilon} + MC^{ef}_{\psi\psi}M^T\right]^{-1}MC^{ef}_{\psi\psi} \tag{127}$$

$$\approx \frac{1}{N-1}\sum_{j=1}^{N}\left(\left(\psi^a\right)_j - \overline{\psi^a}\right)\left(\left(\psi^a\right)_j - \overline{\psi^a}\right)^T \quad . \tag{128}$$

The ensemble covariance matrix $C^{ea}_{\psi\psi}$ of the best estimate does not need to be computed. Nevertheless, comparing Eq. (128) to Eq. (127) may be useful to check Eq. (123) for implementation bugs and convergence of the ensemble.
The Kalman gain $C^{ef}_{\psi\psi}M^T\left[C_{\epsilon\epsilon} + MC^{ef}_{\psi\psi}M^T\right]^{-1}$ does not have to be explicitly computed. It is more efficient to perform a number of matrix-vector computations from right to left.

Computing the term $MC^{ef}_{\psi\psi}M^T$ requires $\mathcal{O}(mn^2)$ multiplications. It is more efficient to compute the dyadic product from Eq. (122):

$$MC^{ef}_{\psi\psi}M^T = \frac{1}{N-1}M\left[\sum_{j=1}^{N}\left(\left(\psi^f\right)_j - \overline{\psi^f}\right)\left(\left(\psi^f\right)_j - \overline{\psi^f}\right)^T\right]M^T \tag{129}$$

$$= \frac{1}{N-1}\sum_{j=1}^{N}\left[M\left(\left(\psi^f\right)_j - \overline{\psi^f}\right)\right]\left[M\left(\left(\psi^f\right)_j - \overline{\psi^f}\right)\right]^T \quad . \tag{130}$$

This requires $\mathcal{O}(Nm^2)$ multiplications. Furthermore, the computation of the sum may be parallelized. A call to `MPI_Allreduce` makes the term $MC^{ef}_{\psi\psi}M^T$ available on all CPU.
The term $C^{ef}_{\psi\psi}M^T$ may also be decomposed into a dyadic product:

$$C^{ef}_{\psi\psi}M^T = \frac{1}{N-1}\left[\sum_{j=1}^{N}\left(\left(\psi^f\right)_j - \overline{\psi^f}\right)\left(\left(\psi^f\right)_j - \overline{\psi^f}\right)^T\right]M^T \tag{131}$$

$$= \frac{1}{N-1}\sum_{j=1}^{N}\left(\left(\psi^f\right)_j - \overline{\psi^f}\right)\left[M\left(\left(\psi^f\right)_j - \overline{\psi^f}\right)\right]^T \quad . \tag{132}$$

The dot product of $M\left(\left(\psi^f\right)_j - \overline{\psi^f}\right)$ and $\left[C_{\epsilon\epsilon} + MC^{ef}_{\psi\psi}M^T\right]^{-1}\left(d_i - M\left(\psi^f\right)_i\right)$ gives a scalar. The vector $\left(\left(\psi^f\right)_j - \overline{\psi^f}\right)$ is multiplied with the scalar. The computation of the sum may again be parallelized. A call to `MPI_Reduce` makes the term $C^{ef}_{\psi\psi}M^T\left[C_{\epsilon\epsilon} + MC^{ef}_{\psi\psi}M^T\right]^{-1}\left(d_i - M\left(\psi^f\right)_i\right)$ available on each CPU. In summary, the procedure is as follows:

1. Compute $d_i - M\left(\psi^f\right)_i$ on each CPU i.
2. Compute $\overline{\psi^f}$ (`MPI_Allreduce`).
3. Compute $\left(\psi^f\right)_j - \overline{\psi^f}$ on each CPU j.
4. Compute $C_{\epsilon\epsilon} + MC^{ef}_{\psi\psi}M^T$ (`MPI_Allreduce`).
5. Solve $\left(C_{\epsilon\epsilon} + MC^{ef}_{\psi\psi}M^T\right)b_i = d_i - M\left(\psi^f\right)_i$ for b_i on each CPU i (`LAPACK`), and collect all b_i on all CPU (`MPI_Allgatherv`).
6. Compute the dot products of $M\left(\left(\psi^f\right)_j - \overline{\psi^f}\right)$ and all b_i on each CPU j.
7. Compute $C^{ef}_{\psi\psi}M^Tb_i$ on each CPU i (`MPI_Reduce`).

Minimum-Norm Least-Squares Problem.
The ensemble covariance matrix $C^{ef}_{\psi\psi}$ of the model prediction is of rank $N-1$, and so is the m-by-m matrix $MC^{ef}_{\psi\psi}M^T$. Depending on the covariance matrix $C_{\epsilon\epsilon}$ of the measurement, the m-by-m matrix $C_{\epsilon\epsilon} + MC^{ef}_{\psi\psi}M^T$ is potentially singular. If $N \leq m$, the matrix $MC^{ef}_{\psi\psi}M^T$ is rank deficient. In the absence of measurement errors, solving $\left(C_{\epsilon\epsilon} + MC^{ef}_{\psi\psi}M^T\right)b_i = d_i - M\left(\psi^f\right)_i$ becomes a minimum-norm

least-squares problem:

$$\underset{b_i}{\text{minimize}} \quad ||b_i||_2 \tag{133}$$

$$\text{s.t.} \quad ||f(b_i)||_2 = \min_{b_j} ||f(b_j)||_2 \quad , \tag{134}$$

$$f(x) := \left(C_{\epsilon\epsilon} + MC^{ef}_{\psi\psi}M^T\right)x - \left(d_i - M\left(\psi^f\right)_i\right) \quad . \tag{135}$$

Covariance inflation.
Note that a finite ensemble size can cause the covariance to be underestimated, which can lead to covariance collapse [43]. There are a few tricks to avoid this, such as a simple covariance inflation [44, 45]

$$\psi^{a,i} = \overline{\psi^a} + \beta(\psi^{a,i} - \overline{\psi^a}) + \alpha, \tag{136}$$

where β is the multiplicative covariance inflation, which could be a scalar or a matrix, and α is the additive covariance inflation, which is a vector.

6.1.5 Square-Root Algorithm and Implementation

For a consistent analysis scheme, the measurements d_j have to form an ensemble. But only one measurement d is usually available. Thus, the measurement d has to be artificially perturbed. The square-root algorithm is based on the covariance matrix $C^{ea}_{\psi\psi}$ of the best estimate (Eq. (127)), which instead uses the covariance matrix $C_{\epsilon\epsilon}$ of the measurement. This renders the sampling of the measurement d unnecessary [46].
For the square-root algorithm, the derivation of the ensemble Kalman filter (Sec. 6.1.4) is reformulated by combining ensemble members into a single column matrix. Ψ is a n-by-N matrix whose columns are the deviations of the ensemble members $(\psi)_j$ from the ensemble mean $\overline{\psi}$. The analysis scheme given by Eq. (123) becomes

$$\left(\psi^f\right)_j = \overline{\psi^f} + \left(\Psi^f\right)_j \quad , \tag{137}$$

$$\left(\psi^a\right)_j = \overline{\psi^a} + \left(\Psi^a\right)_j \quad , \tag{138}$$

$$\overline{\psi^a} = \overline{\psi^f} + C^{ef}_{\psi\psi}M^T\left[C_{\epsilon\epsilon} + MC^{ef}_{\psi\psi}M^T\right]^{-1}\left(d - M\overline{\psi^f}\right) \quad . \tag{139}$$

The ensemble covariance matrices given by Eq. (122) and (128) become

$$C^{ef}_{\psi\psi} \approx \frac{1}{N-1}\Psi^f\left(\Psi^f\right)^T \quad , \tag{140}$$

$$C^{ea}_{\psi\psi} \approx \frac{1}{N-1}\Psi^a\left(\Psi^a\right)^T \quad . \tag{141}$$

Substituting Eq. (140) into Eq. (127) gives

$$C^{ea}_{\psi\psi} = \frac{1}{N-1}\Psi^f\left[1 - \left(M\Psi^f\right)^T\left[(N-1)C_{\epsilon\epsilon} + M\Psi^f\left(M\Psi^f\right)^T\right]^{-1}M\Psi^f\right]\left(\Psi^f\right)^T \tag{142}$$

$$= \frac{1}{N-1}\Psi^f\left[1 - S^TC^{-1}S\right]\left(\Psi^f\right)^T \quad , \tag{143}$$

where

$$S = M\Psi^f \quad , \quad C = (N-1)C_{\epsilon\epsilon} + M\Psi^f\left(M\Psi^f\right)^T \quad . \tag{144}$$

Comparing Eq. (141) with Eq. (143) gives a realization Ψ^a of the ensemble. The task becomes to decompose the right-hand side of Eq. (143). The matrix $S^T C^{-1} S$ on the right-hand side of Eq. (143) is symmetric. As such, it may be decomposed into an orthogonal matrix V and a diagonal matrix Σ. The diagonal matrix Σ is expected to consist of $\min(M, N-1)$ ones with the rest being zeroes. Substituting the decomposition into Eq. (143) gives

$$C^{ea}_{\psi\psi} = \frac{1}{N-1} \Psi^f \left[1 - V \Sigma V^T\right] \left(\Psi^f\right)^T \tag{145}$$

$$= \frac{1}{N-1} \Psi^f V \left[1 - \Sigma\right] \left(\Psi^f V\right)^T \quad . \tag{146}$$

The matrix $1 - \Sigma$ is symmetric and non-negative. Comparing Eq. (146) to Eq. (141) gives a realization Ψ^a of the ensemble:

$$\Psi^a = \Psi^f V \left[1 - \Sigma\right]^{\frac{1}{2}} V^T \quad . \tag{147}$$

The square-root algorithm derives its name from the decomposition of $(N-1)C^{ea}_{\psi\psi}$ into $\Psi^a \left(\Psi^a\right)^T$. Note that Eq. (147) gives a different ensemble than sampling from $C^{ea}_{\psi\psi}$ because the columns of Ψ^a remain in the vector space spanned by the columns of Ψ^a.
The computation of $\overline{\psi^a}$ is implemented as follows:

1. Compute $\overline{\psi^f}$ (`MPI_Allreduce`).
2. Compute $\left(\psi^f\right)_j - \overline{\psi^f}$ on each CPU j.
3. Compute Ψ^f on root (`MPI_Gatherv`).
4. Compute $C_{\epsilon\epsilon} + M C^{ef}_{\psi\psi} M^T$ on root.
5. Compute $d - M\overline{\psi^f}$ on root.
6. Solve $\left(C_{\epsilon\epsilon} + M C^{ef}_{\psi\psi} M^T\right) b = d - M\overline{\psi^f}$ on root (`LAPACK`), and send b to all CPU (`MPI_Bcast`).
7. Compute the dot products of $M\left(\left(\psi^f\right)_j - \overline{\psi^f}\right)$ and b on each CPU j.
8. Compute $C^{ef}_{\psi\psi} M^T b$ on each CPU i (`MPI_Allreduce`).

The computation of Ψ^a is implemented as follows:

1. Solve $\left(C_{\epsilon\epsilon} + M C^{ef}_{\psi\psi} M^T\right) B = M\Psi^f$ on root (`LAPACK`).
2. Compute $S^T C^{-1} S$ on root (`LAPACK`), and send it to all CPU (`MPI_Bcast`).
3. Decompose $C^{ef}_{\psi\psi} M^T b$ into its eigenvalues Σ and eigenvectors V on each CPU i (`LAPACK`).
4. Take the square root of $1 - S^T C^{-1} S$ (`MPI_Allgatherv`).
5. Compute $\left(\Psi^f V \left[1 - \Sigma\right]^{\frac{1}{2}} V^T\right)_i$ on each CPU i (`MPI_Reduce`).

6.1.6 Exercise: Sequential data assimilation in a chaotic system

Use the Lorenz system with $\rho = 28$, $\sigma = 10$ and $\beta = 8/3$.

1. Integrate the equations from the initial condition $[1, 1, 1]$ to 40 time units. Plot the solution in the phase space and the time series of the components.

2. Change the initial condition to $[1, 1, 1 + \epsilon]$ where $\epsilon = 10^{-3}$. Explain the different behaviour.

3. Create an ensemble of two simulations with $C_{\psi\psi,(ij)} = 0.1^2\delta_{ij}$. Take the initial condition from a normal distribution. Plot as before the two overlapped simulations and the error. How long do the trajectories take to diverge from each other?

4. Implement the ensemble Kalman filter with 100 samples, 1000 time steps from one assimilation to the next, observation covariant matrix $C_{\epsilon\epsilon,ij} = 0.1^2\delta_{ij}$ and a measurement matrix equal to the identity.

5. Repeat with the square-root Kalman filter. What is the effect of this filter?

6.2 Sequential data assimilation with Bayesian filtering and smoothing

Parts of this section are adapted from [2].

Data assimilation is here treated as a problem in Bayesian inference, where existing knowledge is quantified in the form of a probability distribution over candidate solutions. When external data becomes available, the probability distribution is updated, effectively combining the existing knowledge with the data.
Data assimilation and parameter estimation are here treated as problems in statistical inference. Statistical inference quantifies the degree of belief (or confidence) in a physical model, the parameters that it receives and the states that it predicts. Statistical inference follows a probabilistic formulation, which provides precise definitions for the different tasks addressed in inference, which include filtering, smoothing and prediction. Probabilistic formulations for statistical inference include *frequentist* inference and *Bayesian* inference. In frequentist inference, an error functional is defined to measure the statistical distance between a candidate solution and the available data. Most of the times, the error functional is conveniently a sum of squares, and subject to Tikhonov regularization to make the problem less ill-posed. Although both inference frameworks may give equivalent results under certain conditions [42], all derivations here are based on Bayes' rule. Inference becomes an optimization problem to minimize this error functional. In Bayesian inference, existing knowledge is quantified in the form of a probability distribution over candidate solutions. When data becomes available, the probability distribution is updated, effectively combining the existing knowledge with the data. For normal distributions under linear dynamics, both formulations of statistical inference give equivalent results [42]. Under these circumstances, frequentist inference may be considered more accessible because it allows the application of familiar tools from convex optimization [47]. Nevertheless, Cox's axioms demonstrate that probability theory, as used in Bayesian inference, gives a natural formulation for inference in the general case [48]. For more details, the reader may refer to [42] or [49].

We recall some basic ingredients of statistical inference and probability theory.

Theorem 1 (Marginalization)**.** *For a joint probability distribution $p(X,Y)$, the marginal probability distributions $p(X)$ and $p(Y)$ are given by*

$$p(X) = \int p(X,Y)\,\mathrm{d}Y \quad , \tag{148}$$

$$p(Y) = \int p(X,Y)\,\mathrm{d}X \quad . \tag{149}$$

Theorem 2 (Bayes' rule)**.** *The conditional probability distributions $p(X \mid Y)$ and $p(Y \mid X)$ are related to the joint probability distribution via*

$$p(X,Y) = p(X)p(Y \mid X) = p(Y)p(X \mid Y) \quad . \tag{150}$$

The conditional probability distribution $p(X \mid Y)$ is sometimes referred to as the inverse of the conditional probability distribution $p(Y \mid X)$. The inverse is given by Bayes' rule:

$$p(X \mid Y) = \frac{p(X,Y)}{p(Y)} = \frac{p(X)p(Y \mid X)}{p(Y)} \quad . \tag{151}$$

If $p(X)$ and $p(Y \mid X)$ are given, $p(Y)$ can be computed through marginalization.

Definition 1 (Normal distribution)**.**

$$\mathcal{N}(x \mid \mu, C) = \frac{1}{\sqrt{(2\pi)^n \det(C)}} \exp\left(-\frac{1}{2}(x-\mu)^T C^{-1}(x-\mu)\right) \tag{152}$$

Corollary 1 (Marginal distribution)**.**

$$p(x) = \mathcal{N}(x \mid \mu, C) \tag{153}$$

$$p(y \mid x) = \mathcal{N}(y \mid Mx + \nu, Q) \tag{154}$$

$$p(y) = \mathcal{N}(y \mid M\mu + \nu, MCM^T + Q) \tag{155}$$

Corollary 2 (Bayes' rule)**.**

$$p(x) = \mathcal{N}(x \mid \mu, C) \tag{156}$$

$$p(y \mid x) = \mathcal{N}(y \mid Mx + \nu, Q) \tag{157}$$

$$p(x \mid y) = \mathcal{N}\left(x \mid \widetilde{\mu}, \widetilde{C}\right) \tag{158}$$

$$\widetilde{\mu} = \mu + (MC)^T (MCM^T + Q)^{-1} \left[y - (M\mu - \nu)\right] \tag{159}$$

$$\widetilde{C} = C - (MC)^T (MCM^T + Q)^{-1} MC \tag{160}$$

In Chapter 6.1, the Kalman filter is derived from an estimator (Eq. (98)). The analysis step gives the statistically optimal estimate given a model prediction and measurements. In this chapter, it is shown that the Kalman filter is a special case of a Bayesian filter. It turns out that the statistically optimal estimate may be interpreted as the maximum-likelihood estimate from a distribution of possible states. In the same way, the Rauch-Tung-Striebel smoother is derived from the Bayesian smoother [50, 49].

6.2.1 Probabilistic state space model

The state of a system at a timestep k is uniquely defined by the state vector x_k. The state vector need not be a scalar or a finite-dimensional tuple, but may be taken from an infinite-dimensional function space. The evolution of the state is governed by a physical model f and its parameters θ. Thus, our belief in the state x_k depends exclusively on our belief in (i) the previous state x_{k-1} as well as our choice of (ii) the physical model f and (iii) its parameters θ. At the same time, the state vector x_k is compared to noisy observations y_k through a measurement operator M. Formulated in terms of a probabilistic state space model, we obtain

$$x_k = x_{k-1} + \int_{t_{k-1}}^{t_k} f(x(t), \theta)\, \mathrm{d}t = G(x_{k-1}, \theta) \sim p(x_k \mid x_{k-1}, \theta, f) \quad , \tag{161}$$

$$y_k = M(x_k) \sim p(y_k \mid x_k) \quad . \tag{162}$$

In brief, the transition from one state to the next is governed by the operator G. The operator G is derived from the physical model f, and depends on the parameters θ. The states x_k and the observations y_k are considered realizations inside their respective probabilistic state spaces. The degrees of belief in each are subject to ("$\sim$") the conditional probability distributions $p(x_k \mid x_{k-1}, \theta, f)$ and $p(y_k \mid x_k)$ respectively. The degree of belief in the state x_k is conditional on the previous state x_{k-1} and the choices in the physical model f and its parameters θ. The degree of belief in the observation y_k is conditional on the true state x_k.

The rules of the probabilistic state space model may be formalized as follows [49]. Firstly, we assume that the physical model may be described by a *Markov chain* [41]. This means that the belief in a state depends only on the belief in the previous state:

1. The future is independent of the past given the present:

$$p(x_k \mid x_{0:k-1}, y_{1:k-1}, \theta, f) = p(x_k \mid x_{k-1}, \theta, f) \quad , \tag{163}$$

where $x_{0:k-1}$ denotes the states at all timesteps from 0 to $k-1$, and $y_{1:k-1}$ denotes the observations at all timesteps from 1 to $k-1$.

2. The past is independent of the future given the present:

$$p(x_k \mid x_{k+1:N}, y_{k+1:N}, \theta, f) = p(x_k \mid x_{k+1}, \theta, f) \quad , \tag{164}$$

where $x_{k+1:N}$ and $y_{k+1:N}$ respectively denote the states and observations at all timesteps from $k+1$ to the final timestep N.

Secondly, observations are assumed to be conditionally independent in time. The probability of an observation depends only on the current state:

$$p(y_k \mid x_{0:N}, y_{1:k-1}, y_{k+1:N}, \theta, f) = p(y_k \mid x_k) \quad . \tag{165}$$

In Fig. 7, the relationship between states and observations is shown as well as the roles of models, parameters and measurement.

The goal of data assimilation is to find the joint probability distribution $p(x_{0:N}, y_{1:N}, \theta, f)$. The probabilistic state space spans all states x_k from timestep 0 to N and all observations y_k from timestep 1 to N, as well as the physical model f and its parameters θ. This joint probability distribution gives a complete statistical description. In principle, all probability distributions of interest may be derived from this joint probability distribution (Table 1). In practice, it is difficult to compute this probability distribution because of the high dimensionality of its probabilistic state space spanning multiple timesteps [51]. Therefore, state estimation focuses on the more direct computation of conditional probability distributions over a single timestep (Table 2).

In the probabilistic formulation, data assimilation is easily extended to account for parameters. In combined state and parameter estimation, the state is augmented by the parameters so that they become subject to the same inference (Eq. (161)):

$$\tilde{x}_k = \begin{pmatrix} x_k \\ \theta_k \end{pmatrix} \quad , \quad \tilde{f}(\tilde{x}(t)) = \begin{pmatrix} f(x(t), \theta_k) \\ 0 \end{pmatrix} \quad , \quad \tilde{x}_k = \tilde{x}_{k-1} + \int_{t_{k-1}}^{t_k} \tilde{f}(\tilde{x}(t))\,\mathrm{d}t \quad . \tag{166}$$

The tasks in combined state and parameter estimation are given in Table 3. The filtered and smoothed distributions in the parameters θ_k, $p(\theta_k \mid y_{1:k}, f)$ and $p(\theta_k \mid y_{1:N}, f)$ respectively, are retrieved by marginalizing the states x_k. Note that the parameters θ_k are now time-dependent as the system traverses different regimes in state space. This turns the strongly constrained parameter estimation into a weakly constrained combined state and parameter estimation [42]. Thus, the results of marginalizing the probability distributions in combined state and parameter estimation (Table 3) are not strictly equivalent to the solutions of parameter estimation (Table 1).

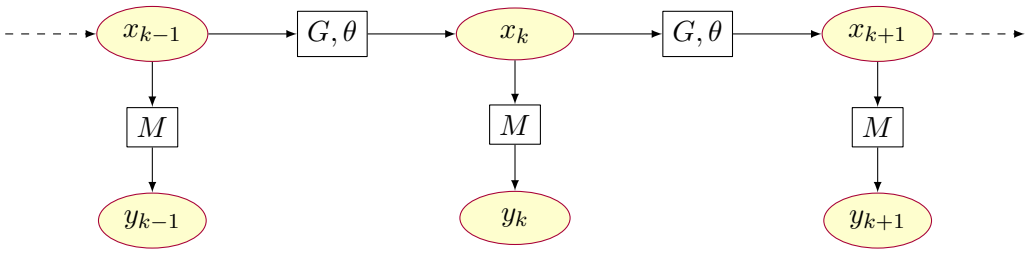

Figure 7: Probabilistic state space model as a Markov chain. The operator G and its parameters θ govern the transition from one state to the next. The state vector x_k is related to the observations y_k through a measurement operator M. From [2].

Table 1: Conditional probability distributions in data assimilation.

Task	PDF	Description
State estimation	$p(x_{0:N} \mid y_{1:N}, \theta, f)$	Given a physical model and its parameters, what is our belief in a series of states?
Parameter estimation	$p(\theta \mid y_{1:N}, f)$	Given a physical model, what is our belief in a set of parameters?
Model comparison	$p(f \mid y_{1:N})$	Between two physical models, in which one do we believe more?

Table 2: Conditional probability distributions in state estimation.

Task	PDF	Description
Filtering	$p(x_k \mid y_{1:k}, \theta, f)$	Given all observations from the past and now, what is our belief in the current state?
Smoothing	$p(x_k \mid y_{1:N}, \theta, f)$	Given all observations from the past, the future and now, what is our belief in the current state?
Prediction	$p(x_{N+1} \mid y_{1:N}, \theta, f)$	Given all observations from the past and now, what is our belief in a future state?

Table 3: Conditional probability distributions in combined state and parameter estimation.

Task	PDF	Description
Filtering	$p(x_k, \theta_k \mid y_{1:k}, f)$	Given all observations from the past and now, what is our belief in the current state and set of parameters?
Smoothing	$p(x_k, \theta_k \mid y_{1:N}, f)$	Given all observations from the past, the future and now, what is our belief in the current state and set of parameters?

6.2.2 Bayesian filtering and smoothing

For the filtering problem, Bayes' rule gives

$$p(x_k \mid y_{1:k}, \theta, f) = \frac{p(y_k \mid x_k, y_{1:k-1}, \theta, f) p(x_k \mid y_{1:k-1}, \theta, f)}{p(y_k \mid y_{1:k-1}, \theta, f)} \tag{167}$$

$$= \frac{p(y_k \mid x_k) p(x_k \mid y_{1:k-1}, \theta, f)}{p(y_k \mid y_{1:k-1}, \theta, f)} \quad . \tag{168}$$

The prediction $p(x_k \mid y_{1:k-1}, \theta, f)$ is given by the Chapman-Kolmogorov equation:

$$p(x_k \mid y_{1:k-1}, \theta, f) = \int p(x_k, x_{k-1} \mid y_{1:k-1}, \theta, f) \, \mathrm{d}x_{k-1} \tag{169}$$

$$= \int p(x_k \mid x_{k-1}, y_{1:k-1}, \theta, f) p(x_{k-1} \mid y_{1:k-1}, \theta, f) \, \mathrm{d}x_{k-1} \tag{170}$$

$$= \int p(x_k \mid x_{k-1}, \theta, f) p(x_{k-1} \mid y_{1:k-1}, \theta, f) \, \mathrm{d}x_{k-1} \quad . \tag{171}$$

The Chapman-Kolmogorov equation requires the inverse from the previous timestep $k-1$. In general, it is solved either numerically [52], analytically (Theorem 5) or by a Monte Carlo simulation (Theorem 6). The steps in the Bayesian filter may be summarized as follows:

Theorem 3 (Bayesian filter)**.**

1. *Prediction step:*

$$p(x_k \mid y_{1:k-1}, \theta, f) = \int p(x_k \mid x_{k-1}, \theta, f) p(x_{k-1} \mid y_{1:k-1}, \theta, f) \, \mathrm{d}x_{k-1} \quad . \tag{172}$$

2. *Update step:*

$$p(x_k \mid y_{1:k}, \theta, f) = \frac{p(y_k \mid x_k) p(x_k \mid y_{1:k-1}, \theta, f)}{p(y_k \mid y_{1:k-1}, \theta, f)} \quad . \tag{173}$$

At the timestep $k = N$, the filtered and smoothed distributions are identical (Tab. 2). If the smoothed distribution at a timestep $k+1$ is known, the smoothed distribution at the previous timestep k is also known due to the Markov chain properties of the probabilistic state space model (Eq. (163), (164)). This may be formalized as follows:

$$p(x_k \mid y_{1:N}, \theta, f) = \int p(x_k, x_{k+1} \mid y_{1:N}, \theta, f) \, \mathrm{d}x_{k+1} \tag{174}$$

$$= \int p(x_k \mid x_{k+1}, y_{1:N}, \theta, f) p(x_{k+1} \mid y_{1:N}, \theta, f) \, \mathrm{d}x_{k+1} \tag{175}$$

$$= \int p(x_k \mid x_{k+1}, y_{1:k}, \theta, f) p(x_{k+1} \mid y_{1:N}, \theta, f) \, \mathrm{d}x_{k+1} \quad . \tag{176}$$

$p(x_{k+1} \mid y_{1:N}, \theta, f)$ is the smoothed distribution from the subsequent timestep $k+1$. $p(x_k \mid x_{k+1}, y_{1:k}, \theta, f)$ is computed via Bayes' rule:

$$p(x_k \mid x_{k+1}, y_{1:k}, \theta, f) = \frac{p(x_{k+1} \mid x_k, y_{1:k}, \theta, f) p(x_k \mid y_{1:k}, \theta, f)}{p(x_{k+1} \mid y_{1:k}, \theta, f)} \tag{177}$$

$$= \frac{p(x_{k+1} \mid x_k, \theta, f) p(x_k \mid y_{1:k}, \theta, f)}{p(x_{k+1} \mid y_{1:k}, \theta, f)} \quad . \tag{178}$$

Note that it involves the filtered distribution from the current timestep k. The steps in the Bayesian smoother may be summarized as follows:

Theorem 4 (Bayesian smoother)**.**

1. *Forward sweep: Bayesian filter (Theorem 3).*
2. *Backward step:*

$$p(x_k \mid y_{1:N}, \theta, f) = p(x_k \mid y_{1:k}, \theta, f) \int \frac{p(x_{k+1} \mid x_k, \theta, f) p(x_{k+1} \mid y_{1:N}, \theta, f)}{p(x_{k+1} \mid y_{1:k}, \theta, f)} \, \mathrm{d}x_{k+1} \quad . \tag{179}$$

Note that both the Bayesian filter and smoother are sequential in nature. In the Bayesian filter, the predicted distribution $p(x_k \mid y_{1:k-1}, \theta, f)$ at a timestep k (Eq. (172)) mainly depends on the filtered distribution $p(x_{k-1} \mid y_{1:k-1}, \theta, f)$ from the previous timestep $k-1$ (Eq. (173)). In the Bayesian smoother, the smoothed distribution $p(x_k \mid y_{1:N}, \theta, f)$ at a timestep k mainly depends on the smoothed distribution $p(x_{k+1} \mid y_{1:N}, \theta, f)$ from the subsequent timestep $k+1$ (Eq. (179)). The existence of sequential algorithms for the computation of filtered and smoothed distributions significantly reduces the complexity of data assimilation [51].

6.2.3 The Kalman filter and the Rauch-Tung-Striebel smoother

Two additional assumptions are introduced to make the computation of filtered and smoothed distributions feasible. Firstly, the prior and the likelihood in the update step of the Bayesian filter are assumed to be normal (Eq. (173)):

$$p(x_k \mid y_{1:k-1}, \theta, f) = \mathcal{N}\left(x_k \mid \psi^f, C^f_{\psi\psi}\right) \quad , \tag{180}$$

$$p(y_k \mid x_k) = \mathcal{N}\left(y_k \mid M x_k, C_{\epsilon\epsilon}\right) \quad , \tag{181}$$

where $\mathcal{N}$ denotes a normal distribution with respective mean and covariance matrix. The mean of the prior is denoted by ψ^f, its covariance matrix by $C^f_{\psi\psi}$, and the covariance matrix of the likelihood, also known as the observation error, by $C_{\epsilon\epsilon}$. From Eq. (180) and (181), it follows that the filtered distribution $p(x_k \mid y_{1:k}, \theta, f)$ is normal (Eq. (173)). Secondly, the operator G (Eq. (161)) in the prediction step (Eq. (172)) is assumed to be linear in x. The result is the well-known Kalman filter [53, 54]:

Theorem 5 (Kalman filter)**.**

$$p(x_k \mid y_{1:k}, \theta, f) = \mathcal{N}\left(x_k \mid \psi^a, C^a_{\psi\psi}\right) \quad , \tag{182}$$

$$\psi^a = \psi^f + \left(M C^f_{\psi\psi}\right)^T \left[C_{\epsilon\epsilon} + M C^f_{\psi\psi} M^T\right]^{-1} \left(y_k - M\psi^f\right) \quad , \tag{183}$$

$$C^a_{\psi\psi} = C^f_{\psi\psi} - \left(M C^f_{\psi\psi}\right)^T \left[C_{\epsilon\epsilon} + M C^f_{\psi\psi} M^T\right]^{-1} \left(M C^f_{\psi\psi}\right) \quad , \tag{184}$$

where the superscript f denotes 'forecast' (everything pertaining to the prediction), and the superscript a denotes 'analysis' (everything pertaining to the update).

If the physical model is nonlinear, the prediction of the covariance matrix $C^f_{\psi\psi}$ for the Kalman filter may be generalized in several ways. In the extended Kalman filter, the predicted covariance matrix $C^f_{\psi\psi}$ is computed by linearizing f [55]. In strongly nonlinear dynamical systems, the predictions are found to be poor [42]. Higher-order extended Kalman filters are available [56]. Nevertheless, drawbacks include their significant storage requirements, which increase exponentially with the order of approximation. An alternative is the ensemble Kalman filter [39, 40]. Instead of a mean ψ and a covariance matrix $C_{\psi\psi}$, a distribution is represented by a sample $\left(\psi^j\right)_{j=1\ldots n}$. During the prediction step, the ensemble members ψ^j evolve in time independently. Before the update step, the statistics may be recovered from the sample as follows:

$$\overline{\psi} \approx \frac{1}{n} \sum_{j=1}^{n} \psi^j \quad , \quad \Psi = \left(\psi^1 - \overline{\psi} \quad , \quad \psi^2 - \overline{\psi} \quad , \quad \cdots \quad , \quad \psi^n - \overline{\psi}\right) \quad , \quad C_{\psi\psi} \approx \frac{1}{n-1} \Psi \Psi^T \quad . \tag{185}$$

The sample covariance matrix $C_{\psi\psi}$ involves division by $n-1$ instead of n in order to avoid a sample bias. Various implementations of the ensemble Kalman filter exist, which differ in the update step. In the straightforward implementation of the ensemble Kalman filter [39], every ensemble member is individually updated (Eq. (183)). It can be shown that the observations must be randomly perturbed in order to guarantee a statistically consistent analysis scheme [40]. In order to avoid the introduction of randomly generated numbers, the square-root filter is used here [57]. The square-root filter belongs to a larger family of ensemble Kalman filters called ensemble-transform Kalman filters [58, 59]. Unlike the straightforward implementation of the ensemble Kalman filter, the mean and the deviations of the ensemble members are updated. This requires the singular value decomposition of a symmetric, positive, semi-definite matrix ($V\Sigma V^T$, where V is orthonormal and Σ diagonal), but no spurious errors due to the random perturbation of the observations are introduced.

Theorem 6 (Square-root filter)**.**

$$(\psi^a)^j = \overline{\psi^a} + (\Psi^a)_j \quad , \tag{186}$$

$$\overline{\psi^a} = \overline{\psi^f} + \Psi^f \left(M\Psi^f\right)^T \left[(n-1)C_{\epsilon\epsilon} + M\Psi^f \left(M\Psi^f\right)^T\right]^{-1} \left(y_k - M\overline{\psi^f}\right) \quad , \tag{187}$$

$$\Psi^a = \Psi^f V \left[\mathbb{I} - \Sigma\right]^{\frac{1}{2}} V^T \quad , \quad V\Sigma V^T = \left(M\Psi^f\right)^T \left[(n-1)C_{\epsilon\epsilon} + M\Psi^f \left(M\Psi^f\right)^T\right]^{-1} M\Psi^f \quad , \tag{188}$$

where $\mathbb{I}$ is the identity matrix.

Following Eq. (180) and (181), the Bayesian smoother (Theorem 4) becomes the Rauch-Tung-Striebel smoother, also known as Kalman smoother (Theorem 7). It can be shown that the smoothed distribution becomes a normal distribution with mean ψ^s and covariance matrix $C^s_{\psi\psi}$. In order to again avoid the shortcomings of assuming linearity, an ensemble Kalman smoother is presented here (Theorem 8).

Theorem 7 (Rauch-Tung-Striebel smoother)**.**

$$p(x_k \mid y_{1:k}) = \mathcal{N}\left(x_k \mid \psi^s, C^s_{\psi\psi}\right) \quad , \tag{189}$$

$$\psi^s = \psi^a + \left(\left(C^f_{\psi\psi}\right)^{-1}_{k+1} G C^a_{\psi\psi}\right)^T \left[\psi^s_{k+1} - \psi^f_{k+1}\right] \quad , \tag{190}$$

$$C^s_{\psi\psi} = C^a_{\psi\psi} - \left(\left(C^f_{\psi\psi}\right)^{-1}_{k+1} G C^a_{\psi\psi}\right)^T \left[\left(C^f_{\psi\psi}\right)_{k+1} - \left(C^s_{\psi\psi}\right)_{k+1}\right] \left(\left(C^f_{\psi\psi}\right)^{-1}_{k+1} G C^a_{\psi\psi}\right) \quad . \tag{191}$$

Proof. Dynamic model with noise (Eq. (109)):

$$p(x_{k+1} \mid x_k) = \mathcal{N}\left(x_{k+1} \mid Gx_k, \overline{q_k q_k^T}\right) \tag{192}$$

Kalman filter:

$$p(x_k \mid y_{1:k}) = \mathcal{N}\left(x_k \mid \psi^a, C^a_{\psi\psi}\right) \tag{193}$$

Apply Bayes' rule using Eq. (192) and (193):

$$p(x_k \mid x_{k+1}, y_{1:k}) = \mathcal{N}\left(x_k \mid \psi^+, C^+_{\psi\psi}\right) \tag{194}$$

$$\psi^+ = \psi^a + \left(\left(C^f_{\psi\psi}\right)^{-1}_{k+1} G C^a_{\psi\psi}\right)^T \left[x_{k+1} - \psi^f_{k+1}\right] \tag{195}$$

$$C^+_{\psi\psi} = C^a_{\psi\psi} - \left(\left(C^f_{\psi\psi}\right)^{-1}_{k+1} G C^a_{\psi\psi}\right)^T \left(C^f_{\psi\psi}\right)_{k+1} \left(\left(C^f_{\psi\psi}\right)^{-1}_{k+1} G C^a_{\psi\psi}\right) \tag{196}$$

Marginalize a joint probability distribution using Eq. (193), (192) at timestep $k+1$:

$$p(x_{k+1} \mid y_{1:T}) = \mathcal{N}\left(x_{k+1} \mid \psi^s_{k+1}, \left(C^s_{\psi\psi}\right)_{k+1}\right) \tag{197}$$

$$p(x_k \mid y_{1:k}) = \mathcal{N}\left(x_k \mid \psi^s, C^s_{\psi\psi}\right) \tag{198}$$

□

Theorem 8 (Ensemble Kalman smoother)**.**

$$(\psi^s)^j = (\psi^a)^j + \Psi^a \big(\Psi^f\big)^{-1}_{k+1} \left[(\psi^s)^j_{k+1} - \Big(\psi^f\Big)^j_{k+1} \right] \quad . \tag{199}$$

Proof. Using pseudoinverses (Section 6.1.4):

$$\psi^s = \psi^a + \left((C^f_{\psi\psi})^{-1}_{k+1} G C^a_{\psi\psi} \right)^T \left[\psi^s_{k+1} - \psi^f_{k+1} \right] \tag{200}$$

$$= \psi^a + \left(\left(\big(\Psi^f\big)_{k+1} \big(\Psi^f\big)^T_{k+1} \right)^{-1} G \big(\Psi^a\big)_k \big(\Psi^a\big)^T_k \right)^T \left[\psi^s_{k+1} - \psi^f_{k+1} \right] \tag{201}$$

$$= \psi^a + \left(\left(\big(\Psi^f\big)_{k+1} \big(\Psi^f\big)^T_{k+1} \right)^{-1} \big(\Psi^f\big)_{k+1} \big(\Psi^a\big)^T_k \right)^T \left[\psi^s_{k+1} - \psi^f_{k+1} \right] \tag{202}$$

$$= \psi^a + \left(\left(\big(\Psi^f\big)^T_{k+1} \right)^{-1} \big(\Psi^a\big)^T_k \right)^T \left[\psi^s_{k+1} - \psi^f_{k+1} \right] \tag{203}$$

$$= \psi^a + \big(\Psi^a\big)_k \big(\Psi^f\big)^{-1}_{k+1} \left[\psi^s_{k+1} - \psi^f_{k+1} \right] \quad . \tag{204}$$

Numerical implementation:

$$\psi^s = \psi^a + \big(\Psi^a\big)_k \left[\big(\Psi^f\big)^T_{k+1} \big(\Psi^f\big)_{k+1} \right]^{-1} \big(\Psi^f\big)^T_{k+1} \left[\psi^s_{k+1} - \psi^f_{k+1} \right] \quad . \tag{205}$$

□

A Path-ordered integrals and the Dyson expansion

The (Schrödinger-like) linear differential equation with variable coefficients

$$2\pi \mathrm{i} He \mathbf{A}(\eta)\hat{\boldsymbol{\mathcal{I}}} = \frac{d\hat{\boldsymbol{\mathcal{I}}}}{d\eta}, \tag{206}$$

where $\mathbf{A}$ is a matrix, $\hat{\boldsymbol{\mathcal{I}}}$ is the solution and He is a number. If the commutator of $\mathbf{A}$ is nil, i.e., $[\mathbf{A}(\eta_1), \mathbf{A}(\eta_2)] = \mathbf{A}(\eta_1)\mathbf{A}(\eta_2) - \mathbf{A}(\eta_2)\mathbf{A}(\eta_1) = 0$, for example when $\mathbf{A}$ is a scalar or a constant matrix, the solution of (206) is $\hat{\boldsymbol{\mathcal{I}}} = \exp\left(2\pi \mathrm{i} He \int_{\eta_a}^{\eta} \mathbf{A}(\eta')d\eta'\right)\hat{\boldsymbol{\mathcal{I}}}_a$, where $\exp(\cdot)$ is the matrix exponential. However, if the commutator is not zero, the matrix-exponential solution no longer holds, because $\exp(\mathbf{A}(\eta_1))\exp(\mathbf{A}(\eta_2)) \neq \exp(\mathbf{A}(\eta_1) + \mathbf{A}(\eta_2))$. A solution for this case is derived by asymptotic expansion. The differential equation (206) is recast in integral form as

$$\hat{\boldsymbol{\mathcal{I}}}(\eta) = \hat{\boldsymbol{\mathcal{I}}}_a + 2\pi \mathrm{i} He \int_{\eta_a}^{\eta} \mathbf{A}(\eta')\hat{\boldsymbol{\mathcal{I}}}(\eta')d\eta', \tag{207}$$

which enables an explicit expression for the solution by recursion. First, the case $He = 0$ is solved. From (206), the solution $\hat{\boldsymbol{\mathcal{I}}}_a$ is constant and is equal to its value at the boundary a. Second, by using He as the perturbation parameter, the solution is expanded as

$$\hat{\boldsymbol{\mathcal{I}}} = \hat{\boldsymbol{\mathcal{I}}}_a + \sum_{n=1}^{\infty} He^n \hat{\boldsymbol{\mathcal{I}}}_n. \tag{208}$$

The asymptotic decomposition (208) is substituted into (206) and, using (207) by recursion, a solution is derived as follows

$$\hat{\boldsymbol{\mathcal{I}}}(\eta) = \underbrace{\left[\mathbb{1} + 2\pi \mathrm{i} He \int_{\eta_a}^{\eta} d\eta^{(1)} \mathbf{A}\left(\eta^{(1)}\right) + \ldots + (2\pi \mathrm{i} He)^n \int_{\eta_a}^{\eta} d\eta^{(1)} \ldots \int_{\eta_a}^{\eta^{(n-1)}} d\eta^{(n)} \mathbf{A}\left(\eta^{(1)}\right) \ldots \mathbf{A}\left(\eta^{(n)}\right)\right]}_{\text{Propagator, } \mathbf{U} = \mathbb{1} + \sum_{n=1}^{\infty} (2\pi \mathrm{i} He)^n \mathbf{P}_n} \hat{\boldsymbol{\mathcal{I}}}_a, \tag{209}$$

where $\eta_a < \eta^{(n)} < \ldots < \eta^{(1)} < \eta$, and $\mathbb{1}$ is the identity operator. The integral operators in (209) are path-ordered, which means that the operator closer to the boundary, $\eta = \eta_a$, is always on the right of the operator acting at a farther location. Equation (209) contains the Neumann series of the acoustic propagator $\mathbf{U} = \mathbb{1} + \sum_{n=1}^{\infty} (2\pi \mathrm{i} He)^n \mathbf{P}_n$, defined as the map such that $\hat{\boldsymbol{\mathcal{I}}}(\eta) = \mathbf{U}(\eta)\hat{\boldsymbol{\mathcal{I}}}_a$. Although asymptotic, solution (209) is absolutely convergent in a finite spatial domain and when $\mathbf{A}$ is bounded. This can be shown by defining the path-ordering operator $\mathcal{P}(\mathbf{P}(\eta_1), \mathbf{P}(\eta_2)) = \mathbf{P}(\eta_1)\mathbf{P}(\eta_2)$ if $\eta_1 > \eta_2$ and $\mathcal{P}(\mathbf{P}(\eta_1), \mathbf{P}(\eta_2)) = \mathbf{P}(\eta_2)\mathbf{P}(\eta_1)$, if $\eta_2 > \eta_1$. After some algebra, it can be shown that [60, 61]

$$\hat{\boldsymbol{\mathcal{I}}} = \mathcal{P}\left(2\pi \mathrm{i} He \int_{\eta_a}^{\eta} \exp\left(\mathbf{A}\left(\eta'\right)\right) d\eta'\right)\hat{\boldsymbol{\mathcal{I}}}_a, \tag{210}$$

which means that

$$\|\hat{\boldsymbol{\mathcal{I}}}\| < \exp\left(\int_{\eta_a}^{\eta} d\eta' \|\mathbf{A}(\eta')\|\right) \|\hat{\boldsymbol{\mathcal{I}}}_a\| < \infty \tag{211}$$

is absolutely convergent. In time-dependent perturbations of quantum systems, the acoustic solution (209) has an analogy to the Dyson series, while the integrands have analogies to the Feynman path integrals [62].

B Ergodic and hyperbolic systems

An ergodic system has the property that

$$\langle \mathcal{J} \rangle_\infty \equiv$$
$$\lim_{T\to\infty} T^{-1} \int_0^T \mathcal{J}(\mathbf{x}; s) dt = \int_\Omega \mathcal{J}(\mathbf{x}; s)\mu(\mathbf{x}; s) d\mathbf{x} \quad \text{for almost all } \mathbf{x}, \tag{212}$$

where $\int_\Omega \mu d\mathbf{x} = 1$ is the the ergodic measure and Ω is the phase space. The ergodic measure is an invariant measure because it is preserved by the action of the function[5]. Equation (212) states that in ergodic systems the average over the phase space is the same as the time-average along one single trajectory for almost every initial condition. "Almost" means that there exists a countable set of initial conditions for which the statement does not hold. Regions of the phase space with large values of μ will be visited by the solutions more often the regions with small values of μ.

A strange attractor is hyperbolic if there is a splitting of the tangent space into stable, neutral and unstable subspaces at every point of the trajectory, $\bar{\boldsymbol{q}}(t)$. Formally, $\mathcal{T}_{\bar{\boldsymbol{q}}} = E^s_{\bar{\boldsymbol{q}}} \oplus E^n_{\bar{\boldsymbol{q}}} \oplus E^u_{\bar{\boldsymbol{q}}}$, where $E^s_{\bar{\boldsymbol{q}}}$ and $E^u_{\bar{\boldsymbol{q}}}$ are the stable and unstable subspaces of dimension N^s and N^u, defined by the directions along which the derivative contracts and expands, respectively, and $E^n_{\bar{\boldsymbol{q}}}$ is the one-dimensional neutral subspace. (Consequently, a quasi-periodic solution is not hyperbolic because it has at least two zero Lyapunov exponents, i.e., $E^n_{\bar{\boldsymbol{q}}}$ is at least two-dimensional.) Hyperbolicity has profound implications on the behaviour of a dynamical system. The existence of unstable subspaces gives rise to exponentially diverging trajectories, which in turn gives rise to unpredictable dynamics in the long term. Furthermore, hyperbolicity often implies structural stability of the attractor, i.e. the qualitative behaviour of the attractor does not change if the system is slightly perturbed. In the problem of computing sensitivities, hyperbolicity is crucial because it determines whether the time-averaged cost functional responds smoothly to perturbations to the parameters [10]. Indeed, the most robust sensitivity algorithms [26, 63, 64, 65, 18] rely on the shadowing lemma [27, 66], which is valid only in hyperbolic systems. Importantly, it has been hypothesised by [67, 68] that most physical dynamical systems develop asymptotically on an attracting set, the dynamics of which can be regarded as hyperbolic. This is called the chaotic hypothesis, which stems from the measure theory of turbulence of [10]. We have numerical evidence that some fluid systems behave like hyperbolic systems (bluff body wake), whereas others may not (2D aerofoil). The chaotic conjecture seems to hold in DNS and LES, where statistical quantities typically respond smoothly to grid refinement (when the grid refinement starts from a sufficiently refined grid).

B.1 Preliminaries

Let $\mathcal{M}$ be a Riemannian manifold of finite dimension n equipped on the tangent space $\mathcal{T}_x\mathcal{M}$ of each point $x \in \mathcal{M}$ with the inner product $\langle \cdot, \cdot \rangle_{\mathcal{T}_x}$, and let $\mathcal{F}^t : \mathcal{M} \to \mathcal{M}$ with $t \in \mathcal{I}$ be the evolution operator from t_0 to $t_0 + t$ of an autonomous dynamical system in $\mathcal{M}$. Here, $\mathcal{I}$ denotes the index set and corresponds to $\mathbb{N}_0$ and $\mathbb{R}_{\geq 0}$ for discrete-time and continuous-time dynamics, respectively. Also, let $\mathcal{B}$ denote a σ-algebra on $\mathcal{M}$, and μ be an invariant probability measure under $\mathcal{F}^t$, that is,

$$\text{Probability measure:} \qquad \mu(\mathcal{M}) = 1, \tag{213a}$$
$$\text{Invariant measure:} \qquad \mu\big((\mathcal{F}^t)^{-1}(A)\big) = \mu(A), \quad \forall A \in \mathcal{B} \quad \forall t \in \mathcal{I}, \tag{213b}$$

where $(\mathcal{F}^t)^{-1}(A) := \{x \in \mathcal{M} : \mathcal{F}^t(x) \in A\}$. The triple $(\mathcal{M}, \mathcal{B}, \mu)$ is further assumed to be complete and isomorphic mod 0 to an interval with Lebesgue measure, that is, $(\mathcal{M}, \mathcal{B}, \mu)$ is a standard (Lebesgue-Rokhlin) probability space. We note that $(\mathcal{F}^t)^{-1} : \mathcal{B} \to \mathcal{X} \subset \mathcal{M}$ is different to the backward evolution operator $\mathcal{F}^{-t} : \mathcal{M} \to \mathcal{M}$; which is only well-defined for invertible dynamical systems. Also, Eq. (213a) implies $\mathcal{F}^t$ is a measurable function. The 4-tuple $(\mathcal{M}, \mathcal{B}, \mu, \mathcal{F}^t)$ completely defines a measure-preserving autonomous dynamical system.

[5] I have skipped a lot of interesting math preambles, which are not extremely necessary here.

B.2 Ergodic theorem

Definition 2. A measure-preserving autonomous dynamical system $(\mathcal{M}, \mathcal{B}, \mu, \mathcal{F}^t)$ is *ergodic* if for every $A \in \mathcal{B}$ such that $(\mathcal{F}^t)^{-1}(A) = A$ (i.e. for every invariant set), either $\mu(A) = 0$ or $\mu(A) = 1$. Such μ is usually referred to as an *ergodic invariant probability measure.*

Theorem 9 (Birkhoff Ergodic Theorem). *Let $(\mathcal{M}, \mathcal{B}, \mu, \mathcal{F}^t)$ be ergodic and let $L^1(\mathcal{M}, \mu) \ni h : \mathcal{M} \to \mathbb{R}$ be a real-valued integrable function. Then, for μ-almost every initial condition $x \in \mathcal{M}$,*

$$\lim_{t\to\infty} \frac{1}{t} \int_{(0,t)} (h \circ \mathcal{F}^t)(x) = \int_{\mathcal{M}} h \; d\mu, \tag{214}$$

including the assertion that the integral and the limit on the left-hand side exist.

In other words, in an ergodic system, "time average" is equal to "phase space average" for μ-almost every initial condition. In non-ergodic systems, a similar result holds for μ_A-almost every initial condition $x \in A$ if the right-hand side in Eq. (214) is replaced by $[\mu(A)]^{-1} \int_{\mathcal{M}} h \; d\mu_A$, where $A \in \mathcal{B}$ is a positive μ-measure, invariant set, and μ_A is the probability measure restricted to A. The ergodic theorem as presented above can be considered as a corollary of this more general result.

B.3 Lyapunov exponents

The Lyapunov stability theory studies how infinitesimal perturbations to a measure-preserving (ergodic or non-ergodic) autonomous dynamical system evolve over (continuous or discrete) time, that is, how infinitesimally close initial conditions evolve with respect to each other over time. The expansion or contraction rate of an infinitesimal perturbation in the direction $0 \neq \xi \in \mathcal{T}_x\mathcal{M}$ is given by

$$\gamma(\xi, x, t) := \frac{||D\mathcal{F}^t(x) \; \xi||_{\mathcal{T}_{\mathcal{F}^t(x)}}}{||\xi||_{\mathcal{T}_x}},$$

where $D\mathcal{F}^t(x) : \mathcal{T}_x\mathcal{M} \to \mathcal{T}_{\mathcal{F}^t(x)}\mathcal{M}$ is the (linear) tangent propagator. Also, we say that $D\mathcal{F}^t$ is "μ-$\log^+$-bounded" if

$$\int_{\mathcal{M}} \sup_{t\leq 1} \log^+ ||D\mathcal{F}^t(x)||_B \; d\mu < \infty, \tag{215}$$

where $\log^+ z := \max(0, \log z)$ and

$$||D\mathcal{F}^t(x)||_B := \sup_{||\xi||_{\mathcal{T}_x}=1} ||D\mathcal{F}^t(x) \; \xi||_{\mathcal{T}_{\mathcal{F}^t(x)}}$$

denotes operator norm.

Definition 3. Provided the limit exists, the Lyapunov exponent associated to $x \in \mathcal{M}$ and $0 \neq \xi \in \mathcal{T}_x\mathcal{M}$ is defined as

$$\Lambda(\xi, x) := \lim_{t\to\infty} \frac{1}{t} \ln\big(\gamma(\xi, x, t)\big). \tag{216}$$

Hence, the Lyapunov exponent $\Lambda(\xi, x)$ indicates the asymptotic rate of exponential growth (or decay) of infinitesimal perturbations δx to the system at $x \in \mathcal{M}$ along the direction $\xi \in \mathcal{T}_x\mathcal{M}$, that is,

$$||\delta x(t)||_{\mathcal{T}_{\mathcal{F}^t(x)}} \sim e^{\Lambda(x,\xi)t}.$$

Theorem 10. *Let $(\mathcal{M}, \mathcal{B}, \mu, \mathcal{F}^t)$ be a measure-preserving autonomous dynamical system. If $D\mathcal{F}^t$ is "μ-$\log^+$-bounded" in the sense in Eq. (215), then the limit in Eq. (216) exists, is finite and independent of the choice of norm $||\cdot||_{\mathcal{T}_x}$ for μ-almost every $x \in \mathcal{M}$ and for every $0 \neq \xi \in \mathcal{T}_x\mathcal{M}$. For fixed x, $\Lambda(\xi, x)$ takes at most $m \leq n$ different values, $\Lambda^1(x) > \cdots > \Lambda^m(x)$, and there exists a filtration of the*

tangent space into subspaces $S_i(x)$, $\mathcal{T}_x\mathcal{M} = S_1(x) \supset \cdots \supset S_m(x) \supset S_{m+1}(x) := 0$ *of dimension* $g_i(x) = \dim S_i(x) - \dim S_{i+1}(x)$ *such that if* $\xi \in S_i(x) \backslash S_{i+1}(x)$ *then* $\Lambda(\xi, x) = \Lambda^i(x)$, $i = 1, ..., m$. *Moreover, for all* $t \in \mathcal{I}$, *the Lyapunov exponents and their multiplicities are* $\mathcal{F}^t$*-invariant* $\Lambda^i \circ \mathcal{F}^t = \Lambda^i$, $g_i \circ \mathcal{F}^t = g_i$, *and the filtration is invariant under the dynamics in the sense that* $\big[D\mathcal{F}^t(x)\big]\big(S_i(x)\big) = S_i(\mathcal{F}^t(x))$.

Corollary 1. *In an ergodic system, the Lyapunov exponents are* μ*-almost everywhere constant, that is, there exists* $A \in \mathcal{B}$ *such that* $\mu(A) = 1$ *and* $\Lambda^i(x) = \Lambda^i$, $i = 1, ..., m$, $\forall x \in A$.

Definition 4. Provided the limit exists, we define the *forward Oseledets' operator* $\mathcal{D}^+(x) : \mathcal{T}_x\mathcal{M} \to \mathcal{T}_x\mathcal{M}$ as

$$\mathcal{D}^+(x) := \lim_{t\to\infty} \frac{1}{2t} \ln\big([D\mathcal{F}^t(x)]^* \; [D\mathcal{F}^t(x)]\big), \tag{217}$$

where $*$ denotes the adjoint operator, $\ln(\cdot)$ is given by the functional calculus, and convergence is in operator norm.

We note that, by construction, this is a linear, positive-definite, self-adjoint operator on $\mathcal{T}_x\mathcal{M}$.

Corollary 2. *For* μ*-almost every* $x \in \mathcal{M}$, *the limit in Eq.* (217) *exists and the eigenvalues* $\lambda_i^+(x)$ *of* $\mathcal{D}^+(x)$ *coincide with the Lyapunov exponents, i.e.* $\lambda_i^+(x) = \Lambda^i(x)$. *Furthermore, the multiplicity* $l_i^+(x)$ *of* $\lambda_i^+(x)$ *is equal to the multiplicity of* $\Lambda^i(x)$, *i.e.* $l_i^+(x) = g_i(x)$.

Corollary 3. *If* $\mathcal{F}^t$ *is a diffeomorphism (see footnote* [6]*) and* $D\mathcal{F}^{-t}$ *is "*μ*-*$\log^+$*-bounded" in the sense in Eq.* (215)*, then the backward Oseledets' operator,*

$$\mathcal{D}^-(x) := \lim_{t\to\infty} \frac{1}{2t} \ln\big([D\mathcal{F}^{-t}(x)]^*[D\mathcal{F}^{-t}(x)]\big),$$

converges for μ*-almost every* $x \in \mathcal{M}$, *and its eigenvalues and multiplicities satisfy* $\lambda_i^-(x) = -\Lambda^i(x)$ *and* $l_i^-(x) = g_i(x)$, $i = 1, ..., m$. *Also, for all* $t \in \mathcal{I}$, *the Lyapunov exponents and their multiplicities are* $\mathcal{F}^{-t}$*-invariant* $\Lambda^i \circ \mathcal{F}^{-t} = \Lambda^i$, $g_i \circ \mathcal{F}^{-t} = g_i$, *and the filtration of the tangent space is invariant under the backward dynamics in the sense that* $\big[D\mathcal{F}^{-t}(x)\big]\big(S_i(x)\big) = S_i(\mathcal{F}^{-t}(x))$.

B.4 Covariant Lyapunov vectors

The covariant Lyapunov vectors (CLVs) are only defined for invertible dynamical systems. For this reason, we shall restrict to this case hereinafter. Also, we will denote the (orthogonal) subspaces spanned by the eigenvectors of $\mathcal{D}^\pm(x)$ by $(U_x^{(i)})^\pm$, $i = 1, ..., m$.

Definition 5. Provided they are well-defined, the Oseledets' subspaces $\Omega_x^{(i)}$ are given by

$$\Omega_x^{(i)} = \big(\Gamma_x^{(i)}\big)^+ \cap \big(\Gamma_x^{(i)}\big)^-, \quad i = 1, ..., m,$$

where

$$\big(\Gamma_x^{(i)}\big)^+ = \big(U_x^{(i)}\big)^+ \cup \cdots \cup \big(U_x^{(m)}\big)^+, \qquad \big(\Gamma_x^{(i)}\big)^- = \big(U_x^{(1)}\big)^- \cup \cdots \cup \big(U_x^{(i)}\big)^-.$$

We note that the Oseledets' subspaces are not orthogonal in general.

Theorem 11. *Let* $\mathcal{F}^t$ *be a diffeomorphism on* $\mathcal{M}$ *such that* $D\mathcal{F}^{\pm t}$ *are "*μ*-*$\log^+$*-bounded" in the sense in Eq.* (215)*. Then, for* μ*-almost every* $x \in \mathcal{M}$, *the Oseledets' subspaces are well-defined, independent of the choice of norm* $||\cdot||_{\mathcal{T}_x}$, *have dimension* $\dim \Omega_x^{(i)} = g_i(x)$, *and form a measurable splitting of the tangent space* $\mathcal{T}_x\mathcal{M} = \Omega_x^{(1)} \oplus \cdots \oplus \Omega_x^{(m)}$. *Furthermore, they satisfy*

$$\lim_{t\to\pm\infty} \frac{1}{t} \ln ||D\mathcal{F}^t(x)\ \xi||_{\mathcal{T}_{\mathcal{F}^t(x)}} = \Lambda^i(x), \qquad \forall 0 \neq \xi \in \Omega_x^{(i)},$$

[6] Let $\mathcal{M}$ and $\mathcal{N}$ be smooth manifolds. A differentiable map $\mathcal{F}^t : \mathcal{M} \to \mathcal{N}$ is called a *diffeomorphism* if it is a bijection and its inverse, denoted by $\mathcal{F}^{-t}$, is differentiable as well.

$$\lim_{t\to\pm\infty}\frac{1}{t}\ln\sin\left(\angle(\Omega^{(i)}_{\mathcal{F}^t(x)},\Omega^{(j)}_{\mathcal{F}^t(x)})\right),\qquad \forall i\neq j,$$

and are invariant under the forward and backward dynamics in the sense that $\left[D\mathcal{F}^{\pm t}(x)\right]\left(\Omega^{(i)}_x\right)=\Omega^{(i)}_{\mathcal{F}^{\pm t}(x)}$ *for all* $t\in\mathcal{I}$.

All the pieces are finally in place to formally introduce the covariant Lyapunov vectors:

Definition 6. A set $\{\psi^j\}_{j=1,\dots,n},\ \psi^j:\mathcal{M}\to\mathcal{T}_x\mathcal{M}$, is a set of covariant Lyapunov vectors if it admits a partition consisting of bases for the m Oseledets' subspaces for every $x\in\mathcal{M}$ in which these subspaces are well-defined.

From this definition and the previous results, several remarks follow:

- The CLVs form a basis of the tangent space $\mathcal{T}_x\mathcal{M}$ μ-almost everywhere.
- The CLVs are such that any infinitesimal perturbation δx along the direction $\psi^j(x)$ will remain along $\psi^j(\mathcal{F}^t(x))$ for all $t\in\mathcal{I}$. Also, the magnitude of the perturbation increases or decreases exponentially at a rate $||\delta x(t)||_{\mathcal{T}_{\mathcal{F}^t(x)}}\sim||\delta x(0)||_{\mathcal{T}_x}\ e^{\Lambda^j(x)t}$ as $t\to\infty$, where $\Lambda^j(x)=\Lambda^j$ μ-almost everywhere in ergodic systems.
- Unlike the Lyapunov exponents, the CLVs are a function of x even in ergodic systems.
- If all the Lyapunov exponents have multiplicity one (i.e. $m=n$) and the system is ergodic, the set of CLVs is unique (up to normalization constant).

We note that the notion of CLVs can be generalized to non-invertible transformations by restricting $\mathcal{F}^t$ to one "branch" of the inverse dynamics. We shall omit the details here. Also, all the results in this appendix hold more generally if $D\mathcal{F}^t(x)$ is replaced by an arbitrary cocycle $\mathcal{A}(t,x)$ on $\mathcal{M}$ (see footnote [7]). Since it is the particular case $\mathcal{A}(t,x)=D\mathcal{F}^t(x)$ that leads to the definition of Lyapunov exponents and covariant vectors, all the theorems have been written in terms of $D\mathcal{F}^t$ to simplify the discussion.
Remark: The eigenvectors of the forward and backward Oseledets' operators coincide with the asymptotic right and left singular vectors of $DL^t(x)$ as $t\to\infty$ and $t\to-\infty$, respectively. Also, while the right/left singular vectors converge, the left/right vectors may not and thus $DL^t(x)$ may not converge as operator. (In fact, the range space of $DL^t(x)$, i.e., $\mathcal{T}_{L^t(x)}\mathcal{M}$, in which the left/right vectors are defined, may even be time dependent.)

[7] Let $(\mathcal{M},\mathcal{B},\mu,\mathcal{F}^t)$ be a measure-preserving autonomous dynamical system. A measurable map $\mathcal{A}:\mathcal{I}\times\mathcal{M}\to GL(s,\mathbb{R})$ is called a *cocycle* if it satisfies $\mathcal{A}(0,x)=I_s$ and $\mathcal{A}(t_1+t_2,x)=\mathcal{A}\big(t_2,\mathcal{F}^{t_1}(x)\big)\ \mathcal{A}(t_1,x),\ \forall x\in\mathcal{M},\ \forall t_1,t_2\in\mathcal{I}$, where $GL(s,\mathbb{R})$ denotes the set of $s\times s$ invertible real matrices and I_s is the $s\times s$ identity matrix.

References

[1] L. Magri and N. A.K. Doan. Physics-informed data-driven prediction of turbulent reacting flows with Lyapunov analysis and sequential data assimilation. In Heinz Pitsch and Antonio Attili, editors, *Data analysis in direct numerical simulation of turbulent combustion*. Springer, 2019.

[2] H. Yu, M. P. Juniper, and L. Magri. Combined State and Parameter Estimation in Level-Set Methods. *Journal of Computational Physics*, pages 1–51, 2019.

[3] H. Yu, T. Jaravel, M. Juniper, M. Ihme, and L. Magri. Data assimilation and optimal calibration in nonlinear models of flame dynamics. *Journal of Engineering for Gas Turbines and Power*, 2019.

[4] Francisco Huhn and Luca Magri. Stability , sensitivity and optimisation of chaotic acoustic oscillations. *Journal of Fluid Mechanics*, 882:A24, 2020.

[5] Tullio Traverso and Luca Magri. Data assimilation in a nonlinear time-delayed dynamical system with Lagrangian optimization. In *International Conference on Computational Science*, pages 156–168. Springer, 2019.

[6] Nathan Baker, Steven Lee, Frank Alexander, Timo Bremer, Aric Hagberg, Yannis Kevrekidis, Habib Najm, Manish Parashar, Abani Patra, James Sethian, Stefan Wild, and Karen Willcox. Basic Research Needs for Scientific Machine Learning: Core Technologies for Artificial Intelligence. Technical report, USDOE Office of Science (SC) (United States), feb 2019.

[7] Karthik Duraisamy, Gianluca Iaccarino, and Heng Xiao. Turbulence Modeling in the Age of Data. *Annual Review of Fluid Mechanics*, 51:357–377, 2019.

[8] Steven L Brunton, Bernd R Noack, and Petros Koumoutsakos. Machine Learning for Fluid Mechanics. *Annual Review of Fluid Mechanics*, 52(1), 2019.

[9] E. N. Lorenz. Atmospheric Predictability as Revealed by Naturally Occurring Analogues. *Journal of the Atmospheric Sciences*, 26(4):636–646, 1969.

[10] David Ruelle. Ergodic Theory of Differentiable Dynamical Systems. *Publications mathematiques de l'IHES*, 50(1):27–58, 1979.

[11] J. P. Eckmann and D. Ruelle. Ergodic theory of chaos and strange attractors. *Reviews of Modern Physics*, 57:617–656, 1985.

[12] G. Boffetta, M. Cencini, M. Falcioni, and A. Vulpiani. Predictability: a way to characterize complexity. *Physics Reports*, 356:367–474, 2002.

[13] I. Goldhirsch, P.-L. Sulem, and S. A. Orszag. Stability and Lyapunov stability of dynamical systems: A differential approach and a numerical method. *Physica D: Nonlinear Phenomena*, 27(3):311–337, 1987.

[14] P. J. Blonigan, P. Fernandez, S. M. Murman, Q. Wang, G. Rigas, and L. Magri. Towards a chaotic adjoint for LES. In *Center for Turbulence Research, Summer Program*, 2016.

[15] G. Nastac, J.W. Labahn, L. Magri, and M. Ihme. Lyapunov exponent as a metric for assessing the dynamic content and predictability of large-eddy simulations. *Physical Review Fluids*, 2(9):094606, 2017.

[16] Prakash Mohan, Nicholas Fitzsimmons, and Robert D. Moser. Scaling of Lyapunov Exponents in Homogeneous Isotropic Turbulence. *Physical Review Fluids*, 2:114606, 2017.

[17] P. Fernandez and Q. Wang. Lyapunov spectrum of the separated flow around the NACA 0012 airfoil and its dependence on numerical discretization. *Journal of Computational Physics*, 350:453–469, 2017.

[18] A. Ni and Q. Wang. Sensitivity analysis on chaotic dynamical systems by Non-Intrusive Least Squares Shadowing (NILSS). *Journal of Computational Physics*, 347:56–77, 2017.

[19] Malik Hassanaly and Venkat Raman. Ensemble-LES analysis of perturbation response of turbulent partially-premixed flames. *Proceedings of the Combustion Institute*, 37(2):2249–2257, 2019.

[20] Valery Iustinovich Oseledets. A multiplicative ergodic theorem. Characteristic Ljapunov, exponents of dynamical systems. *Trudy Moskovskogo Matematicheskogo Obshchestva*, 19:179–210, 1968.

[21] Francesco Ginelli, Hugues Chaté, Roberto Livi, and Antonio Politi. Covariant Lyapunov vectors. *Journal of Physics A: Mathematical and Theoretical*, 46(25), 2013.

[22] Anatole Katok and Boris Hasselblatt. *Introduction to the modern theory of dynamical systems*, volume 54. Cambridge university press, 1997.

[23] F. Ginelli, P. Poggi, A. Turchi, H. Chat\'e, R. Livi, and A. Politi. Characterizing dynamics with covariant lyapunov vectors. *Physical Review Letters*, 99(13):130601, 2007.

[24] J. Guckenheimer and P. Holmes. *Nonlinear oscillations, dynamical systems, and bifurcations of vector fields*. Springer-Verlag New York, 1983.

[25] L. Magri. Adjoint methods as design tools in thermoacoustics. *Applied Mechanics Reviews*, 71(2):020801, 2019.

[26] Q. Wang and J. Gao. The drag-adjoint field of a circular cylinder wake at Reynolds numbers 20, 100 and 500. *Journal of Fluid Mechanics*, pages 145–161, 2012.

[27] Rufus Bowen and David Ruelle. The ergodic theory of Axiom A flows. *Inventiones Mathematicae*, 29:181–202, 1975.

[28] É. Blayo, M. Bocquet, E. Cosme, and L. F. Cugliandolo. *Advanced Data Assimilation for Geosciences*. Oxford University Press, first edition, 2015.

[29] T. C. Lieuwen and V. Yang. *Combustion Instabilities in Gas Turbine Engines: Operational Experience, Fundamental Mechanisms, and Modeling*. American Institute of Aeronautics and Astronautics, Inc., Reston, VA 20191-4344, USA, 2005.

[30] M. P. Juniper. Triggering in the horizontal Rijke tube: non-normality, transient growth and bypass transition. *Journal of Fluid Mechanics*, 667:272–308, nov 2011.

[31] A. Orchini, G. Rigas, and M. P. Juniper. Weakly nonlinear analysis of thermoacoustic bifurcations in the Rijke tube. *Journal of Fluid Mechanics*, 805:523–550, 2016.

[32] L. Crocco. Research on combustion instability in liquid propellant rockets. *Symposium (International) on Combustion*, 12(1):85–99, 1969.

[33] Ben T. Zinn and Manuel E. Lores. Application of the Galerkin Method in the Solution of Non-linear Axial Combustion Instability Problems in Liquid Rockets. *Combustion Science and Technology*, 4(1):269–278, 1971.

[34] L. D. Landau and E. M. Lifshitz. *Fluid Mechanics*. Pergamon Press, second edition, 1987.

[35] K. I. Matveev and F. E. C. Culick. A model for combustion instability involving vortex shedding. *Combustion Science and Technology*, 175:1059–1083, 2003.

[36] K. Balasubramanian and R. I. Sujith. Thermoacoustic instability in a Rijke tube: Non-normality and nonlinearity. *Physics of Fluids*, 20(4):044103, 2008.

[37] L. Magri and M. P. Juniper. Sensitivity analysis of a time-delayed thermo-acoustic system via an adjoint-based approach. *Journal of Fluid Mechanics*, 719:183–202, 2013.

[38] W. H. Press, S. A. Teukolsky, W. T. Vetterling, and B. P. Flannery. *Numerical recipes*. Cambridge University Press, 3rd edition, 2007.

[39] Geir Evensen. Sequential data assimilation with a nonlinear quasi-geostrophic model using Monte Carlo methods to forecast error statistics. *Journal of Geophysical Research*, 99(C5):10143, 1994.

[40] Gerrit Burgers, Peter Jan van Leeuwen, and Geir Evensen. Analysis scheme in the ensemble Kalman filter. *Monthly Weather Review*, 126(6):1719–1724, June 1998.

[41] Arnaud Doucet, Nando Freitas, and Neil Gordon, editors. *Sequential Monte Carlo Methods in Practice*. Springer New York, 2001. doi: 10.1007/978-1-4757-3437-9.

[42] Geir Evensen. *Data Assimilation - The Ensemble Kalman Filter*. Springer, 2009.

[43] Peter Jan van Leeuwen. Comment on "Data Assimilation Using an Ensemble Kalman Filter Technique". *Monthly Weather Review*, 127(6):1374–1377, 2002.

[44] Jeffrey L. Anderson and Stephen L. Anderson. A Monte Carlo Implementation of the Nonlinear Filtering Problem to Produce Ensemble Assimilations and Forecasts. *Monthly Weather Review*, 127(12):2741–2758, 2002.

[45] Jeffrey S. Whitaker and Thomas M. Hamill. Evaluating Methods to Account for System Errors in Ensemble Data Assimilation. *Monthly Weather Review*, 140(9):3078–3089, 2012.

[46] R N Bannister. A Square-Root Ensemble Kalman Filter Demonstration with the Lorenz model, 2012.

[47] Stephen P. Boyd and Lieven Vandenberghe. *Convex Optimization*. Cambridge University Press, 2004.

[48] Edwin T Jaynes. *Probability theory: The logic of science*. Cambridge university press, 2003.

[49] Simo Särkkä. *Bayesian filtering and smoothing*, volume 3. Cambridge University Press, 2013.

[50] Andrew H Jazwinski. *Stochastic processes and filtering theory*. Courier Corporation, 2007.

[51] Richard Bellman. *Dynamic programming*. Dover Publications, 2003. OCLC: 834140800.

[52] Desmond J. Higham. An Algorithmic Introduction to Numerical Simulation of Stochastic Differential Equations. *SIAM Review*, 43(3):525–546, January 2001.

[53] R. E. Kalman. A New Approach to Linear Filtering and Prediction Problems. *Journal of Basic Engineering*, 82(1):35, 1960.

[54] R. E. Kalman and R. S. Bucy. New Results in Linear Filtering and Prediction Theory. *Journal of Basic Engineering*, 83(1):95, 1961.

[55] Arthur Gelb, editor. *Applied optimal estimation*. MIT Press, 1974.

[56] Robert N. Miller, Michael Ghil, and François Gauthiez. Advanced data assimilation in strongly nonlinear dynamical systems. *Journal of the Atmospheric Sciences*, 51(8):1037–1056, April 1994.

[57] Jeffrey S. Whitaker and Thomas M. Hamill. Ensemble Data Assimilation without Perturbed Observations. *Monthly Weather Review*, 130(7):1913–1924, July 2002.

[58] Michael K. Tippett, Jeffrey L. Anderson, Craig H. Bishop, Thomas M. Hamill, and Jeffrey S. Whitaker. Ensemble Square Root Filters. *Monthly Weather Review*, 131(7):1485–1490, July 2003.

[59] David M. Livings, Sarah L. Dance, and Nancy K. Nichols. Unbiased ensemble square root filters. *Physica D: Nonlinear Phenomena*, 237(8):1021–1028, June 2008.

[60] C. S. Lam. Decomposition of time-ordered products and path-ordered exponentials. *Journal of Mathematical Physics*, 39(10):5543–5558, 1998.

[61] L. Magri. On indirect noise in multi-component nozzle flows. *Journal of Fluid Mechanics*, 828:R2, 2017.

[62] F. J. Dyson. The radiation theories of Tomonaga, Schwinger, and Feynman. *Physical Review*, 75(3):486–502, 1949.

[63] Patrick J. Blonigan and Qiqi Wang. Least squares shadowing sensitivity analysis of a modified Kuramoto-Sivashinsky equation. *Chaos, Solitons and Fractals*, 64(1):16–25, 2014.

[64] Qiqi Wang. Convergence of the least squares shadowing method for computing derivative of ergodic averages. *SIAM Journal on Numerical Analysis*, 52(1):156–170, 2014.

[65] Patrick J. Blonigan. Adjoint sensitivity analysis of chaotic dynamical systems with non-intrusive least squares shadowing. *Journal of Computational Physics*, 348:803–826, 2017.

[66] Sergei Yu Pilyugin. *Shadowing in dynamical systems*. Springer, 2006.

[67] G. Gallavotti and E. G. D. Cohen. Dynamical ensembles in stationary states. *Journal of Statistical Physics*, 80(5-6):931–970, sep 1995.

[68] Giovanni Gallavotti. Entropy, thermostats, and chaotic hypothesis. *Chaos: An Interdisciplinary Journal of Nonlinear Science*, 16(4):043114, dec 2006.